

**THE STUDY OF CIRRUS CLOUDS USING AIRBORNE AND
SATELLITE DATA**

A Thesis

by

KERRY GLYNNE MEYER

Submitted to the Office of Graduate Studies of
Texas A&M University
in partial fulfillment of the requirements for the degree of
MASTER OF SCIENCE

May 2004

Major Subject: Atmospheric Sciences

**THE STUDY OF CIRRUS CLOUDS USING AIRBORNE AND
SATELLITE DATA**

A Thesis

by

KERRY GLYNNE MEYER

Submitted to Texas A&M University
in partial fulfillment of the requirements
for the degree of

MASTER OF SCIENCE

Approved as to style and content by:

Ping Yang
(Chair of Committee)

Thomas Wilheit
(Member)

George Kattawar
(Member)

Richard Orville
(Head of Department)

May 2004

Major Subject: Atmospheric Sciences

ABSTRACT

The Study of Cirrus Clouds Using Airborne and Satellite Data. (May 2004)

Kerry Glynne Meyer, B.S., Texas A&M University

Chair of Advisory Committee: Dr. Ping Yang

Cirrus clouds are known to play a key role in the earth's radiation budget, yet are one of the most uncertain components of the earth-atmosphere system. With the development of instruments such as the Airborne Visible/Infrared Imaging Spectrometer (AVIRIS) and the Moderate-resolution Infrared Spectroradiometer (MODIS), scientists now have an unprecedented ability to study cirrus clouds. To aid in the understanding of such clouds, a significant study of cirrus radiative properties has been undertaken. This research is composed of three parts: 1) the retrieval of tropical cirrus optical thickness using MODIS level-1b calibrated radiance data, 2) a survey of tropical cirrus cloud cover, including seasonal variations, using MODIS level-3 global daily gridded data, and 3) the simultaneous retrieval of cirrus optical thickness and ice crystal effective diameter using AVIRIS reflectance measurements.

DEDICATION

This manuscript is dedicated to all of my family and friends who have helped and supported me throughout the years.

ACKNOWLEDGEMENTS

I would like to thank my advisor, Dr. Ping Yang, for his guidance, support, ideas, and patience throughout my work on this project. Without his aid, this thesis would never have been finished. I greatly appreciate everything he has done for me, and for the opportunity he has given me to continue my education. Also, I would like to thank the members of my advisory committee, Dr. Thomas Wilheit and Dr. George Kattawar, for showing an interest in my research, and for taking time out of their schedules to assist in editing this manuscript.

I would like to thank Dr. Bo-Cai Gao at the Naval Research Laboratory for his help on my projects and publications. I would like to thank Dr. Bryan Baum and Shaima Nasiri for their help with the DISORT code. I would also like to thank Drs. Michael King and Steve Platnick for the MODIS visualization software developed by their group.

This study was supported by NASA/EOS grant NAG5-11935, and also partially supported by the NASA Radiation Sciences Program managed by Drs. Donald Anderson and Hal Maring (NAG-1-02002), the National Science Foundation Physical Meteorology Program managed by Dr. William A. Cooper (ATM-0239605), and a subcontract (4400053274) from Science Applications International Corporation.

Last but not least, I would like to thank my family and friends, especially my mom, my dad, my brother, and my grandparents, for all of the support they have given me throughout the years. I would also like to thank Alison Gardner, the love of my life, for the loving support and patience she has given me.

TABLE OF CONTENTS

| | Page |
|--|------|
| ABSTRACT..... | iii |
| DEDICATION..... | iv |
| ACKNOWLEDGEMENTS..... | v |
| TABLE OF CONTENTS..... | vi |
| LIST OF FIGURES..... | viii |
| 1. INTRODUCTION..... | 1 |
| 2. METHODOLOGY..... | 5 |
| 2.1 Research Objectives..... | 5 |
| 2.2 DISORT..... | 5 |
| 2.3 MODIS Cirrus Reflectance..... | 8 |
| 3. CIRRUS OPTICAL THICKNESS FROM MODIS LEVEL-1B | |
| REFLECTANCE DATA..... | 16 |
| 3.1 Methodology..... | 16 |
| 3.2 Optical Thickness Retrieval from MODIS Data..... | 23 |
| 3.3 Discussion/Summary..... | 33 |
| 4. SURVEY OF TROPICAL CIRRUS OPTICAL THICKNESS USING MODIS | |
| LEVEL-3 DATA..... | 35 |
| 4.1 Methodology..... | 35 |
| 4.2 Retrieval..... | 36 |
| 4.3 Preliminary Results..... | 37 |
| 4.4 Discussion/Summary..... | 45 |
| 5. CIRRUS OPTICAL THICKNESS AND EFFECTIVE SIZE FROM | |
| AVIRIS DATA..... | 46 |

| | Page |
|---------------------------------|------|
| 5.1 Background..... | 46 |
| 5.2 Method..... | 51 |
| 5.3 Preliminary Results..... | 56 |
| 5.4 Discussion/Summary..... | 71 |
| 6. SUMMARY AND CONCLUSIONS..... | 73 |
| 7. REFERENCES..... | 75 |
| VITA..... | 83 |

LIST OF FIGURES

| FIGURE | Page |
|---|------|
| 1 The atmospheric configuration assumed for the cirrus bi-directional reflectance retrieval in Gao et al..... | 10 |
| 2 Scatter plot of DISORT calculated 0.66 vs. 1.375 μm reflectance values, with linear curve fitting..... | 12 |
| 3 Conceptual illustration of the method for deriving Γ | 13 |
| 4 Sample MODIS images illustrating the method of Gao et al..... | 15 |
| 5 Phase function plots for the 0.66 and 1.375 μm wavelength channels..... | 20 |
| 6 Plot of 0.66 μm reflectance vs. optical thickness from DISORT calculations..... | 22 |
| 7 Terra MODIS level-1b image over the Indian Ocean..... | 25 |
| 8 Retrieved optical thickness of the outlined region in Figure 7 (b)..... | 26 |
| 9 Terra MODIS level-1b image over Africa..... | 28 |
| 10 Retrieved optical thickness of the outlined region in Fig. 9 (b)..... | 29 |
| 11 Terra MODIS level-1b image over the western equatorial Pacific Ocean..... | 31 |
| 12 Retrieved optical thickness images from outlined region in Fig. 11 (b)..... | 32 |
| 13 MODIS level-3 derived isolated cirrus reflectance from Terra satellite on July 27, 2002..... | 38 |
| 14 Tropical cirrus optical thickness derived from MODIS level-3 cirrus reflectance corresponding to Fig. 13..... | 39 |

| FIGURE | Page |
|--|------|
| 15 Total number of days between September 2001 and October 2002 with cirrus optical thickness greater than zero..... | 42 |
| 16 Number of days during the winter months of December, January, and February with cirrus optical thickness greater than zero..... | 43 |
| 17 Number of days during the summer months of June, July, and August with cirrus optical thickness greater than zero..... | 44 |
| 18 Sample AVIRIS images..... | 48 |
| 19 A cirrus reflectance spectrum measured by AVIRIS..... | 49 |
| 20 Mid-latitude cirrus phase functions..... | 54 |
| 21 Sample look-up table for AVIRIS retrieval..... | 55 |
| 22 AVIRIS Scene 1 images..... | 58 |
| 23 Scene 1 AVIRIS 1.38 vs. 1.24 μm scatter plot..... | 59 |
| 24 Scene 1 retrieval images..... | 60 |
| 25 AVIRIS Scene 2 images..... | 63 |
| 26 Scene 2 AVIRIS 1.38 vs. 1.24 μm scatter plot..... | 64 |
| 27 Scene 2 retrieval images..... | 65 |
| 28 AVIRIS Scene 3 images..... | 67 |
| 29 Scene 3 AVIRIS 1.38 vs. 1.24 μm scatter plot..... | 68 |
| 30 Scene 3 retrieval images..... | 69 |

1. INTRODUCTION

The knowledge of the optical properties (cloud optical thickness and ice crystal effective size, in particular) of cirrus clouds is essential to the understanding of the radiation balance and climate feedback associated with cirrus radiative forcing. Cirrus clouds may substantially regulate the long-wave radiative energy exchange in the vicinity of the tropical tropopause, and thus are radiatively important [17], [18]. Thin cirrus clouds near the tropical tropopause occur frequently [47], [43], and have been detected by satellite measurements [36], ground-based lidar [27], and space shuttle-borne lidars [45]. Total cirrus cover has been found to be over 50% for the entire tropics [5], and a thin cirrus layer may be present as much as 80% of the time in this region [42]. On a global scale, thin cirrus clouds are primarily confined to the tropical regions, with a rather sharp frequency of presence over the Western Pacific Ocean, particularly during the northern winter when the tropopause temperature is lowest [35], [21]. Most recently, Dessler and Yang [7] showed that sub-visual cirrus clouds, with optical thickness less than 0.03 [38], are ubiquitous over the tropics.

Cirrus clouds have been studied in some detail, and the general radiative and microphysical properties of such clouds have been inferred and modeled in previous studies [1], [2], [4], [5]. However, despite the facts that tropical cirrus clouds have a significant impact on the local radiation budget and climate, and are ubiquitous near the

This thesis follows the style and format of *IEEE Transactions on Geoscience and Remote Sensing*.

tropical tropopause (over the Western Pacific, in particular), relatively little is known about their spatial and temporal distributions. Relevant studies are hampered by the lack of detailed measurements of the radiative and microphysical properties of these clouds, although recent studies have focused on this issue [30]. In fact, cirrus clouds are one of the most uncertain components in atmospheric research because of their high altitudes, optically thin nature, and the nonsphericity of ice crystals in those clouds.

Optical thickness of cirrus clouds is of major interest in the study of the radiative effects of these clouds. Thick clouds reflect more short-wave radiation to space and trap more long-wave radiation in the atmosphere than thin clouds. Also, ice clouds (i.e., cirrus) reflect and scatter radiation differently than water clouds. Even sub-visual cirrus clouds (i.e., invisible to the naked eye) play a role in the radiation budget, although to what extent is still unknown. An important factor in determining the optical thickness of a cirrus cloud is the effective size of the ice crystals that compose such a cloud. Following the principles of radiative scattering, larger ice crystals scatter more radiation in the forward direction, whereas smaller crystals have less forward scattering and more backscattering. These phenomena play a key role in determining the optical thickness of the cloud. Thus, a significant amount of the current research efforts in the remote sensing community have been focused on quantifying these radiative properties.

One instrument used in the study of cirrus clouds is the Airborne Visible Infrared Imaging Spectrometer (AVIRIS) [40], [16]. The AVIRIS instrument, developed by the NASA Jet Propulsion Laboratory, contiguously covers the spectral region from 0.4 to 2.5 μm , using 224 channels. When viewing from an ER-2 aircraft at an altitude of 20

km, the resolution is approximately $20\text{ m} \times 20\text{ m}$ with a swath width of 12 km. The spatial resolution can be increased even further (with a smaller swath width) at lower altitudes. This instrument is useful in various field campaigns, as well as for data validation. However, data from this instrument is limited to specific areas and times, and does not have a global reach.

Of a somewhat greater importance to the research discussed here is the satellite-borne Moderate-resolution Imaging Spectroradiometer (MODIS). MODIS has a much more extensive view of the earth than does AVIRIS, although at a much lower spatial resolution. It is equipped with 36 spectral bands, and was designed for the studies of the atmosphere, land and ocean [22], [24], [34]. The MODIS instrument is currently a key component of NASA's Earth Observing System (EOS), as it is on board both the Terra and Aqua satellites. From these satellites, at an altitude of 705 km, MODIS has a spatial resolution of 1 km with a viewing swath of 2330 km, and can provide a global coverage within 1 to 2 days. Data from this instrument is used extensively in the research discussed here.

MODIS is the first satellite-borne instrument that features the $1.375\text{ }\mu\text{m}$ channel for the exclusive study of cirrus clouds. The $1.375\text{ }\mu\text{m}$ channel is located in a strong water vapor absorption band; therefore, the $1.375\text{ }\mu\text{m}$ reflectance included in the MODIS level-1b calibrated radiance data set is due essentially to the reflection by high ice clouds, which undergoes relatively little attenuation by the water vapor above these clouds. Unlike the $1.375\text{ }\mu\text{m}$ channel, the solar radiation at a visible wavelength, say, $0.66\text{ }\mu\text{m}$, is reflected by both low- and middle-level clouds composed of water droplets

as well as high clouds composed of ice crystals. For cirrus cloudy conditions, the reflected solar radiation at a visible wavelength is strongly contaminated by the surface reflection. Therefore, the measured $0.66\ \mu\text{m}$ reflectance cannot be considered as the reflectance of cirrus clouds. However, MODIS bands 1 ($0.66\ \mu\text{m}$) and 26 ($1.375\ \mu\text{m}$) can be used together to obtain isolated cirrus reflectance at visible wavelengths ($0.4\ \mu\text{m} < \lambda < 1.0\ \mu\text{m}$) [14]. This method is now an operational MODIS product. This derived cirrus reflectance allows for the independent study of cirrus cloud optical properties.

The study presented here will consist of research devoted to the understanding of the radiative properties of cirrus clouds, as well as the spatial and temporal distributions of such clouds. A general methodology will first be described in Section 2. This section also contains a brief overview of the science background required for the present study. In Section 3, a new method is presented to convert MODIS isolated cirrus reflectance, which is derived using the algorithm of Gao et al. [14], to the corresponding optical thickness for tropical cirrus clouds. A brief survey of the tropical cirrus optical thickness fields is then presented in Section 4. Section 5 introduces a new method for simultaneously retrieving cirrus cloud optical thickness and ice crystal effective diameter from 1.38 and $1.88\ \mu\text{m}$ reflectance. Finally, in Section 6, the conclusions are summarized and discussed. It is hoped that this study helps to address several unresolved issues in the field of atmospheric remote sensing.

2. METHODOLOGY

2.1 Research Objectives

The objectives of the research discussed here are three-fold:

- Cloud optical thickness of tropical cirrus is retrieved using the 0.66- and 1.375 μm MODIS level-1b calibrated radiance data and a simple look-up table approach. All MODIS data are obtained from the data access system at NASA Goddard DAAC.
- A preliminary global survey of tropical cirrus cover is performed using the retrieval code produced in Objective 1. MODIS level-3 daily gridded cirrus reflectance is converted into cirrus optical thickness, which is then compared with the MODIS operational cloud product [24], [34].
- Cirrus optical thickness and ice crystal effective diameter are retrieved simultaneously using AVIRIS 0.66, 1.38, and 1.88 μm reflectance measurements and a simple look-up table approach. The AVIRIS data used in the research presented here are obtained from Dr. Bo-Cai Gao at the Naval Research Laboratory.

2.2 DISORT

The research presented here makes use of the Discrete Ordinates Radiative Transfer (DISORT) model for reflectance calculations and look-up table generation. The DISORT code is a numerical algorithm that models the scattering and emittance of

monochromatic radiation in a layered medium. It is capable of radiative calculations involving wavelengths ranging from the ultraviolet to the microwave region of the spectrum. The equations employed by DISORT are based on the well-known theory of radiative transfer described by Chandrasekhar [3]. Here, we use the DISORT 2.0 Beta algorithm for our calculations, which is available to the public and at the present time is the most current version of the code developed by Stamnes et al. [39].

DISORT calculates the transfer of monochromatic radiation at frequency ν through a plane-parallel medium using

$$\mu \frac{du_\nu(\tau_\nu, \mu, \phi)}{d\tau} = u_\nu(\tau_\nu, \mu, \phi) - S_\nu(\tau_\nu, \mu, \phi), \quad (1)$$

where $u_\nu(\tau_\nu, \mu, \phi)$ is the specific intensity in the (μ, ϕ) direction with optical thickness τ_ν (measured perpendicular to the medium surface), azimuthal angle ϕ , and cosine of the polar angle μ . The source function S_ν is given by

$$S_\nu(\tau_\nu, \mu, \phi) = \frac{\omega_\nu(\tau_\nu)}{4\pi} \int_0^{2\pi} d\phi' \int_{-1}^1 d\mu' P_\nu(\tau_\nu, \mu, \phi; \mu', \phi') \times u_\nu(\tau_\nu, \mu', \phi') + Q_\nu(\tau_\nu, \mu, \phi), \quad (2)$$

where $\omega_\nu(\tau_\nu)$ is the single-scattering albedo and $P_\nu(\tau_\nu, \mu, \phi; \mu', \phi')$ is the phase function.

$Q_\nu(\tau_\nu, \mu, \phi)$ is the internal source term, and is given by

$$Q_\nu(\tau_\nu, \mu, \phi) = Q_\nu^{(thermal)}(\tau_\nu, \mu, \phi) + Q_\nu^{(beam)}(\tau_\nu, \mu, \phi), \quad (3)$$

$$Q_\nu^{(thermal)}(\tau_\nu, \mu, \phi) = [1 - \omega_\nu(\tau_\nu)] B_\nu(T), \text{ and} \quad (4)$$

$$Q_v^{(beam)}(\tau_v, \mu, \phi) = \frac{\omega_v(\tau_v)}{4\pi} I_0 P_v(\tau_v, \mu, \phi; -\mu_0, \phi_0) \times \exp\left(\frac{-\tau_v}{\mu_0}\right), \quad (5)$$

where $Q_v^{(thermal)}(\tau_v, \mu, \phi)$ is the source term for thermal emission in local thermodynamic equilibrium, $Q_v^{(beam)}(\tau_v, \mu, \phi)$ is the source term for a parallel beam incident in direction μ_0, ϕ_0 on a non-emitting medium under the usual diffuse-direct distinction, $B_v(T)$ is the Planck function at temperature T , and I_0 is the incident intensity [39].

In the DISORT method, the scattering phase function is expanded in terms of Legendre polynomials. Because the size of ice crystals is much larger than the wavelength of solar radiation, the corresponding phase function is strongly peaked in the forward direction. For a phase function with a strong forward peak, thousands of Legendre polynomial terms are required in the phase function expansion. In practice, the strong forward peak needs to be truncated, for example, by using the delta-M method [46]. In this study, however, we use the δ -fit method [20], which is an extension of the delta-M method. The δ -fit method uses a least-squares fitting approach to generate the coefficients (c_l) of the Legendre polynomial expansion. The objective is to minimize the relative difference ε between the approximated phase function $P'(\theta_l)$ and the actual phase function $P_{ac}(\theta_l)$:

$$\varepsilon = \sum_i w_i \left(\frac{P'(\theta_i)}{P_{ac}(\theta_i)} - 1 \right)^2, \quad (6)$$

$$P'(\theta_i) = \sum_{l=0}^{N_{\text{str}}} c_l p_l(\cos\theta_i), \quad (7)$$

where θ_i is the scattering angle, w_i is the weight for each scattering angle, $p_l(\cos\theta_i)$ is the l th Legendre polynomial, and N_{str} is the number of streams (expansion terms) needed for the desired accuracy.

The expansion coefficients c_l are calculated by solving the least-squares fitting problem $\partial\varepsilon/\partial c_k = 0$ ($k=0,N$):

$$\sum_{i=0} \frac{p_k(\cos\theta_i)}{P_{ac}(\theta_i)} w_i \left(\sum_{l=0}^{N_{\text{str}}} \frac{c_l p_l(\cos\theta_i)}{P_{ac}(\theta_i)} - 1 \right) = 0. \quad (8)$$

The normalized phase function can then be written as

$$P_{\delta\text{-fit}}(\theta_i) = \frac{1}{1-f} P'(\theta_i). \quad (9)$$

For the studies described here, we use 32 streams to represent the phase function ($N_{\text{str}}=32$). The δ -fit method described here allows for a better estimation of the phase function at large scattering angles than the conventional method [20].

2.3 MODIS Cirrus Reflectance

In this study, the optical thickness look-up library is generated under the assumption of the presence of a single cirrus cloud in a completely transparent atmosphere with no surface reflection. However, reflectance of the visible band contained in level-1b calibrated radiance data from the MODIS instrument on board both the Terra and Aqua

satellites includes both atmospheric and surface effects (which include attenuation, scattering, surface reflectance, etc.). The need arises then to remove these effects from the data in order to match the conditions used in the look-up library.

The method used to remove surface and atmospheric effects from MODIS level 1b data to obtain the “true” cirrus reflectance is described in Gao et al. [14]. First, the atmosphere is assumed to be composed of three distinct layers. The top layer is composed of the water vapor above cirrus clouds (which acts to attenuate both the incoming and reflected radiation), the middle layer contains the cirrus clouds, and the bottom layer consists of low-level water clouds, aerosols, water vapor (which accounts for about 90-99% of the total atmospheric water vapor), and the surface. This bottom layer is classified as the “virtual surface,” which takes into account the effects of absorption and scattering by various gases, water vapor, aerosols below cirrus clouds, and low- and mid-level clouds, as well as surface reflection. Fig. 1 shows the atmospheric configuration assumed here. The “virtual surface,” or, more specifically, the low-level water vapor, acts to absorb most, if not all, of the radiation transmitted through cirrus clouds and surface reflected $1.375\ \mu\text{m}$ radiation. Thus, its effects are considered negligible in the MODIS measurement of $1.375\ \mu\text{m}$ reflectance (i.e., the $1.38\ \mu\text{m}$ reflectance can be considered as only that which is reflected by cirrus clouds). The $0.66\ \mu\text{m}$ radiation, however, is in fact affected by the “virtual surface.” The radiation at this wavelength is able to penetrate through the low-level water vapor, and is then reflected by low-level water clouds and the surface of the earth. In effect, the $0.66\ \mu\text{m}$

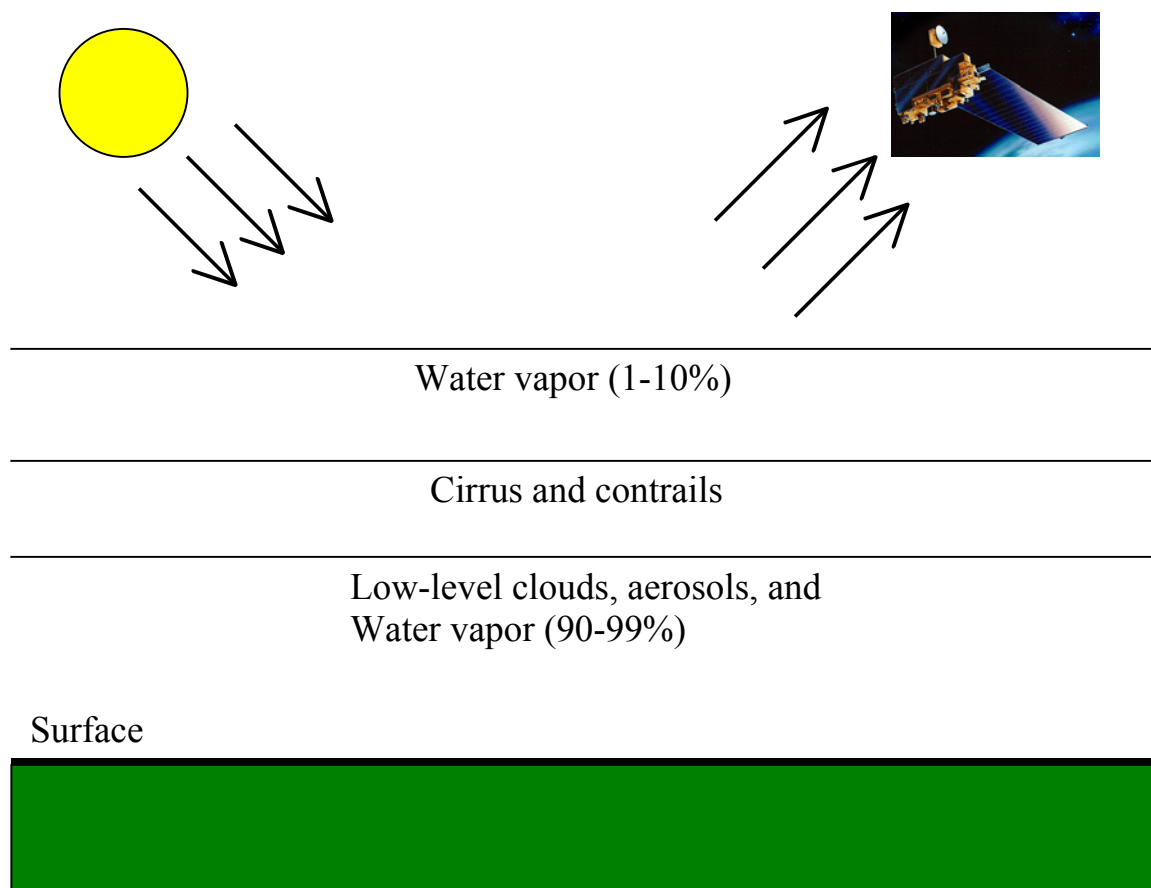


Fig. 1. The atmospheric configuration assumed for the cirrus bi-directional reflectance retrieval in Gao et al. (2002).

reflectance measured by MODIS includes the surface and water cloud reflectance, and cannot be considered solely as the cirrus reflectance.

Previous studies have shown that the relationship between the 0.66 and 1.375 μm cirrus reflectance (without atmospheric and surface effects) is quasi-linear [13], and has a slope smaller than 1 due to weak ice crystal absorption of the 1.375 μm band. Fig. 2 illustrates this correlation using calculated data from DISORT for nine CEPEX size distributions used in this study (these are discussed in Section 3.1.1). The slope of the linear-fit line is indicated at the top of the figure. For MODIS data, cirrus reflectance is coupled with the effects of the atmosphere and the surface. Gao et al. [14] show that the apparent reflectances at MODIS bands 1 and 26 under cirrus cloudy condition are correlated as follows:

$$r_{1.38}(\mu_0, \phi_0, \mu, \phi) = \Gamma r_{0.66}(\mu_0, \phi_0, \mu, \phi) + d, \quad (10)$$

where $r_{1.375}$ and $r_{0.66}$ are the apparent reflectances of the 1.375 and 0.66 μm bands, respectively, Γ is the correlation between the 1.375 and 0.66 μm band apparent reflectance, and d depends on the optical properties of cirrus clouds and the absorption and scattering by various gases, water vapor, aerosols below cirrus clouds, and low- and mid-level clouds, as well as surface reflection. Fig. 3 conceptually illustrates the method for deriving Γ . The isolated cirrus reflectance (without the contamination of surface reflection and atmospheric effects) can then be obtained as follows:

$$r_{c,0.66}(\mu_0, \phi_0, \mu, \phi) = \frac{r_{1.38}(\mu_0, \phi_0, \mu, \phi)}{\Gamma}. \quad (11)$$

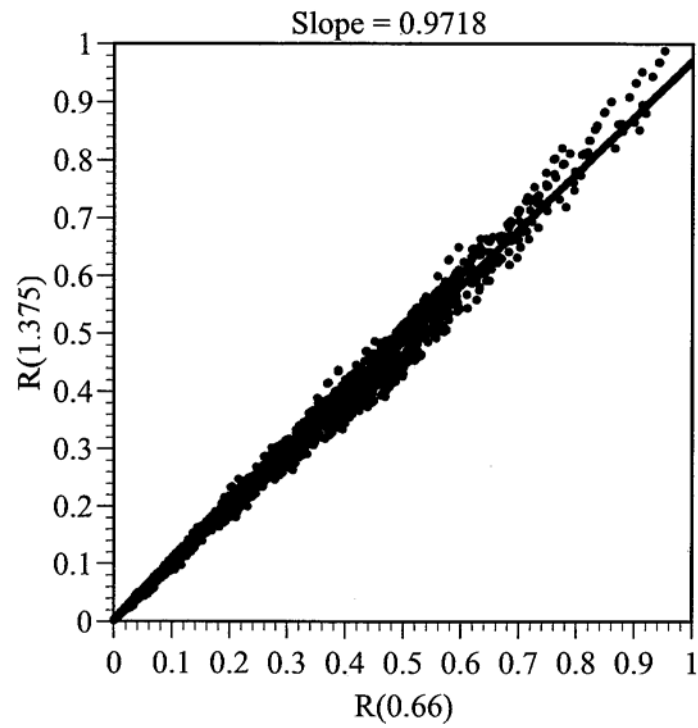


Fig. 2. Scatter plot of DISORT calculated 0.66 vs. 1.375 μm reflectance values, with linear curve fitting.

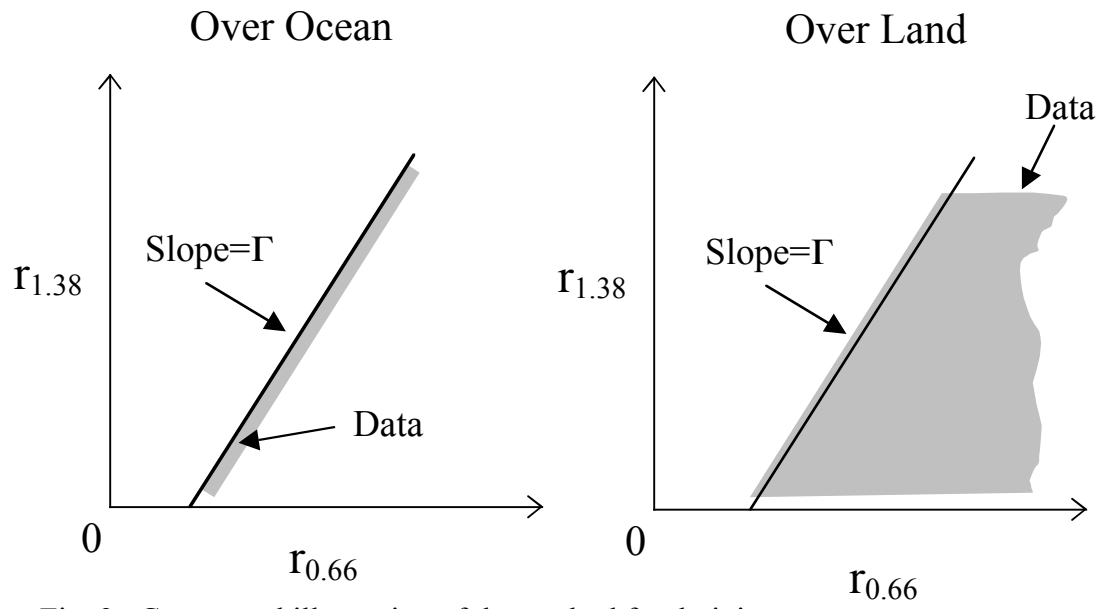


Fig. 3. Conceptual illustration of the method for deriving Γ .

Furthermore, the cirrus reflectance in the visible region has little spectral variation, that is,

$$r_{\lambda}(\mu_0, \phi_0, \mu, \phi) \cong r_{c,0.66}(\mu_0, \phi_0, \mu, \phi), \quad (12)$$

where $0.4 \mu m < \lambda < 1 \mu m$. Therefore, the derivation of cirrus reflectance at visible wavelengths reduces to the determination of the parameter Γ . An algorithm based on MODIS level-1b calibrated band 1 and 26 radiance data has been developed to determine Γ [14], and consequently, the cirrus visible reflectance.

Fig. 4 (a) shows a $0.66 \mu m$ MODIS reflectance image taken over southeastern Asia. The surface and low-level water clouds are clearly visible in this image. Fig. 4 (b) is the corresponding $1.375 \mu m$ MODIS reflectance image. Note the absence of the surface and low-level water clouds. Fig. 4 (c) is the derived visible cirrus reflectance calculated using the cirrus reflectance retrieval algorithm developed by Gao et al. [14]. Note the similarities between Figs. 4 (b) and (c). The optical thickness retrieval algorithm from Section 2.3 has been integrated into the cirrus reflectance algorithm. This combination algorithm is capable of optical thickness retrieval using MODIS level-1b calibrated radiance data on a pixel-by-pixel basis.

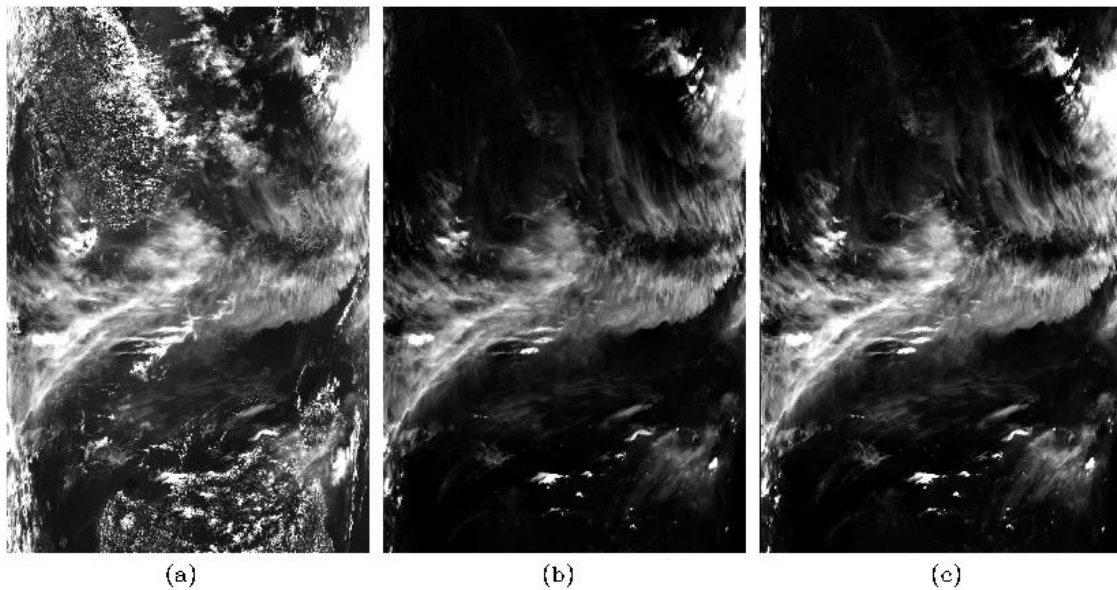


Fig. 4. Sample MODIS images illustrating the method of Gao et al. (a) 0.66 μm channel MODIS image over southeastern Asia. (b) 1.375 μm channel MODIS image corresponding to (a). (c) Derived visible cirrus reflectance corresponding to (a).

3. CIRRUS OPTICAL THICKNESS FROM MODIS LEVEL-1B REFLECTANCE DATA*

3.1 Methodology

The general methodology used to retrieve the optical thickness of tropical cirrus clouds from the MODIS 0.66- μm and 1.375- μm bands essentially follows the physical principle shown by Nakajima and King [32], who found that the reflectance of clouds at a visible channel is sensitive to cloud optical thickness and insensitive to cloud particle size. In the present study, a cirrus optical property database is created first by integrating the single scattering properties of individual ice crystal habits over in-situ observed size distributions and the applicable spectral bands. A representative size distribution is then chosen for the production of an optical thickness look-up table. This look-up table is created using the Discrete Ordinates Radiative Transfer (DISORT) code [39] for an isolated cirrus cloud without including atmospheric absorption. Furthermore, using the algorithm developed by Gao et al. [14], isolated cirrus reflectance at visible wavelengths is then derived by removing the atmospheric effects and surface reflection on the basis of the correlation of MODIS level-1b calibrated band 1 (0.66 μm) and band 26 (1.375 μm) radiance data. Consequently, the optical thickness is derived from a look-up interpolation based on the pre-calculated relationship between optical thickness and cirrus reflectance.

*© 2004 IEEE. Reprinted, with permission, from K. Meyer, P. Yang, and B.-C. Gao, "Optical thickness of tropical cirrus clouds derived from the MODIS 0.66- and 1.375- μm channels," *IEEE Trans. Geosci. Remote Sensing*, 42, 2004.

3.1.1 *Optical Properties Database*

The scattering properties for the individual ice crystal habits used to create the optical properties database are discussed in Yang et al. [49]. The scattering database covers six habits, 56 wavelength channels (0.2-5.0 μm), and 24 size bins (3-4000 μm , in terms of maximum crystal dimension). Tropical cirrus clouds are considered to contain only three of these habits: rough aggregates, solid columns, and bullet rosettes. For the bullet rosette data in this study, spatial bullet rosettes composed of two to six bullet branches randomly oriented in space are used [48]. Intuitively, these three habits vary in concentration from cloud to cloud. However, it is useful to approximate an average habit percentage to describe tropical cirrus in general. The habit percentage used in this study is assumed to be 33.7% solid columns, 24.7% bullet rosettes, and 41.6% aggregates [29].

To integrate the scattering properties with respect to ice crystal size, in-situ observational size distribution data are needed. Here, data obtained during the Central Equatorial Pacific Ocean Experiment (CEPEX) are used. These data were collected from three independent cirrus anvils on March 17, April 1, and April 4, 1993, using an aircraft-borne Particle Measuring System (PMS) two-dimensional cloud probe (2DC) and a video ice particle sampler (VIPS) [19], [28], [10].

Integration of cirrus optical properties is then completed over the nine CEPEX size distributions using previously defined formulas [33]. Calculated properties of interest to this study include the mean effective diameter, extinction coefficient, single-scattering albedo, asymmetry factor, percentage of delta-transmission, truncation energy, and the

associated phase functions and scattering angles. Effective diameter is calculated using the following definition [8], [9], [33]:

$$D_e = \frac{3}{2} \frac{\sum_{D=D_{\min}}^{D_{\max}} \left[\sum_{h=1}^3 V(h,D) f(h,D) n(D) \Delta(D) \right]}{\sum_{D=D_{\min}}^{D_{\max}} \left[\sum_{h=1}^3 A(h,D) f(h,D) n(D) \Delta(D) \right]}, \quad (13)$$

where h is the habit, D is the size bin, $V(h,D)$ is the equivalent volume of each ice crystal, $A(h,D)$ is equivalent area, $f(h,D)$ is the habit percentage, $n(D)$ is the number concentration of ice crystals (from the aforementioned CEPEX data), and $\Delta(D)$ is the bin width. The extinction coefficient and single-scattering albedo are defined as

$$\bar{\beta}_{ext} = \sum_{D=D_{\min}}^{D_{\max}} \left[\sum_{h=1}^3 f(h,D) \sigma_{ext}(h,D) n(D) \Delta(D) \right] \text{ and} \quad (14)$$

$$\bar{\omega}_o = \frac{\bar{\sigma}_{sca}}{\bar{\sigma}_{ext}}, \quad (15)$$

where $\sigma_{ext}(h,D)$ is the extinction cross section of each crystal, and $\bar{\sigma}_{sca}$ and $\bar{\sigma}_{ext}$ are the mean scattering and extinction cross sections, respectively. The phase function at scattering angle Θ is given by

$$\bar{P}(\Theta) = \frac{\sum_{D=D_{\min}}^{D_{\max}} \left[\sum_{h=1}^3 f(h,D) P(\Theta, h, D) \sigma_{sca}(h, D) n(D) \Delta(D) \right]}{\sum_{D=D_{\min}}^{D_{\max}} \left[\sum_{h=1}^3 f(h,D) \sigma_{sca}(h, D) n(D) \Delta(D) \right]}, \quad (16)$$

where σ_{sca} is the scattering cross section of each crystal [33].

Fig. 5 shows the bulk scattering phase function at different effective sizes at wavelengths $0.66\ \mu\text{m}$ and $1.375\ \mu\text{m}$ for tropical cirrus clouds (the different curves in the plot indicate different size distributions, i.e. different effective sizes). The nine size distributions of cirrus clouds in CEPEX (effective diameters ranging from $17.7\ \mu\text{m}$ to $128.8\ \mu\text{m}$) were used in the figure. The habit and percentage of ice particles are illustrated on the top of the figure. Evidently, the phase functions are strongly forward-peaked. The 22° and 46° scattering maxima corresponding to halos are associated with the hexagonal structure of the particles. The detailed features of the scattering phase function and associated physical mechanisms can be found in Yang and Liou [48] and Macke et al. [26].

3.1.2 Optical Thickness Look-up Library

In this study, the $0.66\ \mu\text{m}$ visible band and the $1.375\ \mu\text{m}$ “cirrus detection” band [13] are used first to derive the isolated cirrus bi-directional reflectance (at visible wavelengths) free of surface reflection and atmospheric effects [14]. To retrieve the optical thickness of tropical cirrus clouds, a correlation between cirrus reflectance and optical thickness must be established. This is accomplished using the DISORT code

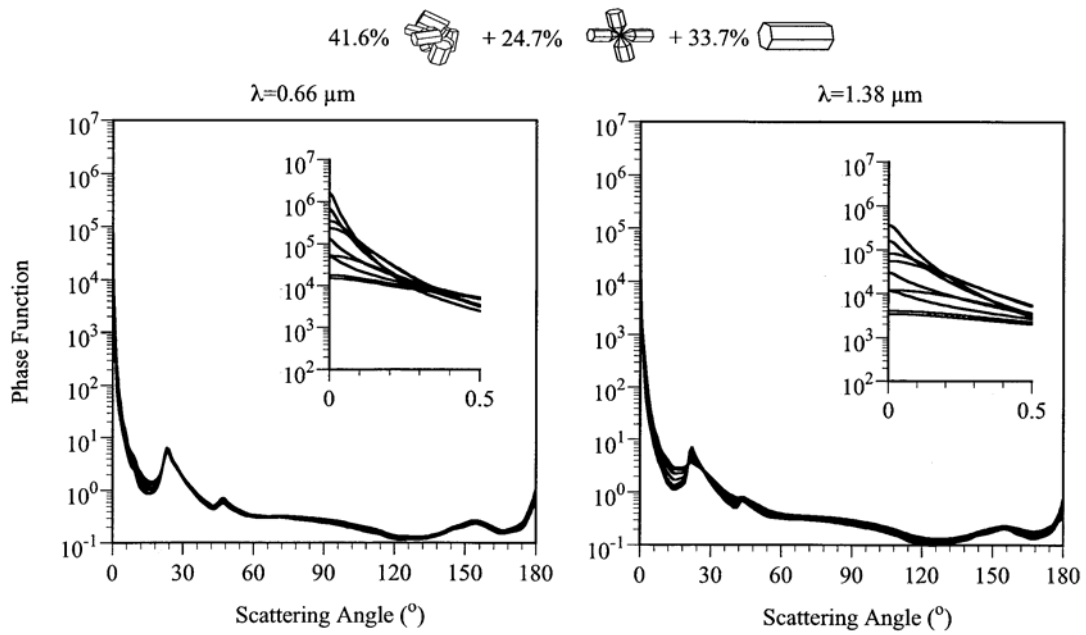


Fig. 5. Phase function plots for the 0.66 and 1.375 μm wavelength channels. The habits used in this study are also shown above.

to model the radiative effects of an isolated cirrus cloud on the solar wavelengths of interest. Scattering data from the previously calculated optical properties database is used as input for each DISORT run. DISORT is first run using all nine tropical cirrus cases (effective diameters ranging from 17.7 to 128.1 μm) for optical depths ranging from 0.002 to 20.0. A limited number of viewing geometries (solar and viewing zenith angles, and relative azimuth angles) are used for comparison purposes. This run allows the determination of the correlation between the cirrus reflectance for each wavelength and the optical thickness of the cloud.

Fig. 6 shows the correlation between 0.66 μm reflectance and optical thickness for four independent viewing geometries. Reflectance of the 0.66 μm wavelength is found to be quite sensitive to the optical thickness of the cloud, but is not sensitive to ice crystal size because of the negligible absorption of ice at this wavelength, as evident from the refractive index of ice [44]. It is therefore possible to retrieve the optical depth of a given tropical cirrus cloud by using the cirrus reflectance at the 0.66 μm wavelength channel. The relatively small reflectance deviation between the smallest and largest effective diameters in Fig. 6 indicates little sensitivity to crystal size. With these results, a single CEPEX size distribution can be selected to use as a representative case to generate the look-up library. For this study, the median size distribution ($D_e = 34.97$ μm) has been chosen.

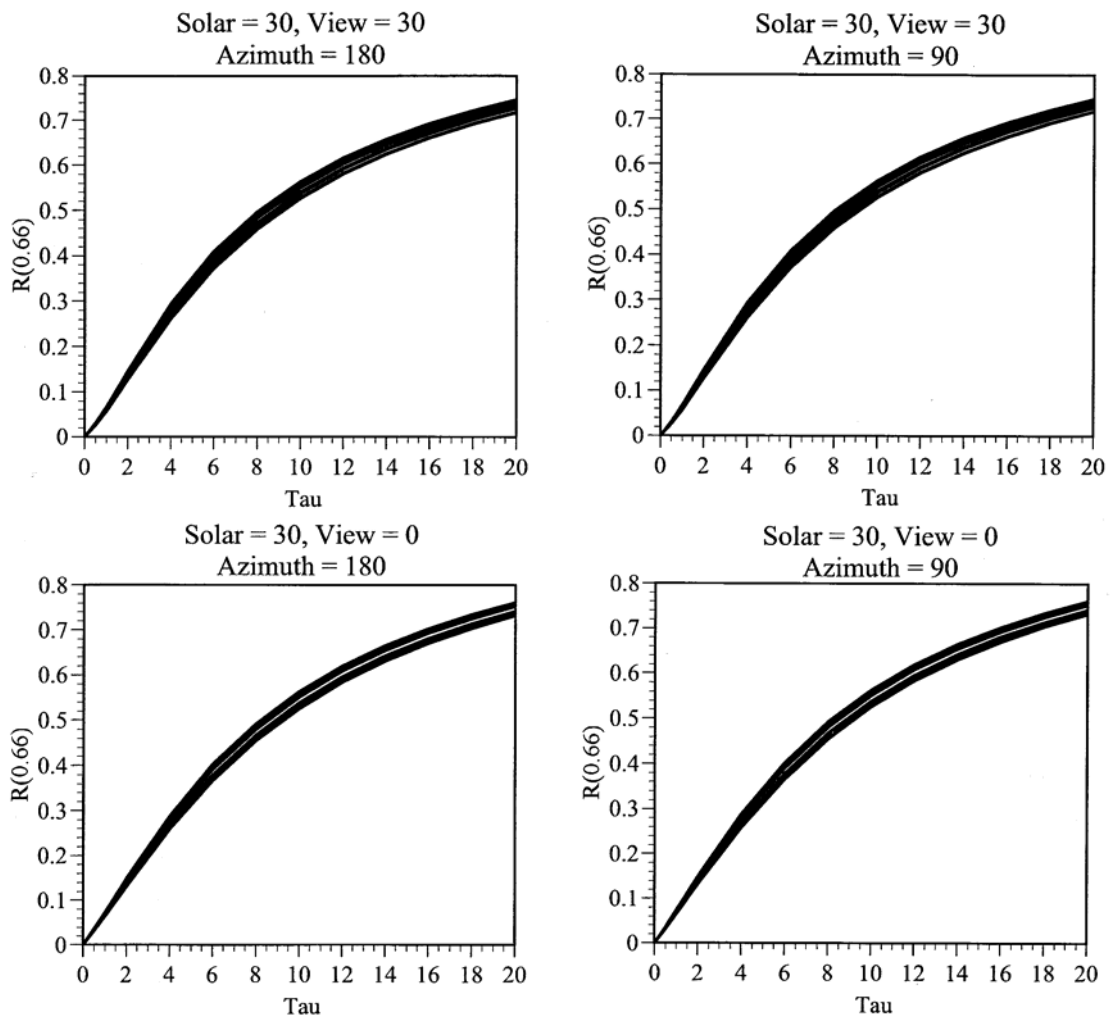


Fig. 6. Plot of 0.66 μm reflectance vs. optical thickness from DISORT calculations (effective diameters from 17.7 μm to 128.1 μm).

The DISORT code is run using 4864 solar and satellite viewing geometries, with solar and viewing zenith angles from 0 to 75° (five degree intervals), and relative azimuth angles from 0 to 180° (ten degree intervals). Input optical depths range from 0.002 to 100.0 (optical depths between 0.0 and 0.002 are assumed to have a linear relationship with the corresponding 0.66 μm reflectance values, allowing for the retrieval of sub-visual cirrus). The resulting look-up library consists of the 0.66 μm cirrus reflectance and the optical depths for each solar and satellite-view geometry used in the retrieval. An algorithm has been developed to interpolate the optical thickness of a given cirrus cloud from the look-up library using only the solar and view zenith angle, the relative azimuth angle, and the corresponding 0.66 μm cirrus reflectance value as input.

3.2 Optical Thickness Retrieval from MODIS Data

To demonstrate the effectiveness of the algorithm and methods discussed in Section 3.1, we apply the cirrus reflectance and optical thickness retrieval algorithm to MODIS data from the Terra satellite. Here, the publicly available 0.66 and 1.375 μm (MODIS channels 1 and 26, respectively) level-1b calibrated radiance data are used. These data have 1 km spatial resolution, and have been processed to sensor units and are radiometrically corrected and geolocated. A normal granule of MODIS level-1b data has a size of 1354 \times 2030 pixels. Due to the shape of the earth as well as the orientation of the beam swath, individual pixel size varies throughout the granule. Pixels at nadir in the MODIS granule are generally square in shape, while pixels at the “eastern” and

“western” sides are not square and are larger in size. However, this irregularity does not affect the retrieval of optical thickness in this study.

The retrieval algorithm has been developed to first retrieve the isolated visible cirrus reflectance for a single MODIS granule. The optical thickness is then interpolated from the reflectance data and the optical thickness look-up table. The algorithm itself is written to interpolate the optical thickness at each individual pixel in the MODIS granule (2748620 total pixels per granule). Intuitively, this is extremely CPU intensive (it takes more than 15 minutes to complete the retrieval for a single MODIS granule on a workstation). However, this approach has the ability to retrieve the optical thickness of tropical cirrus clouds (including those which are optically thin, and are thus invisible) in great detail.

In this study, the retrieval algorithm has been applied to two individual MODIS granules to demonstrate its flexibility: one over the ocean and the other over land. Fig. 7 (a) is a visible MODIS image (using the 0.66 μm wavelength channel) from the Terra satellite over the Indian Ocean on July 13, 2002. Low-level water clouds are prevalent throughout the image, most notably on the bottom and right sides. Scattered cumulus lines are also visible. However, blow-off cirrus clouds are clearly visible in the central regions. For this granule, this region of blow-off cirrus is the area of focus for the retrieval.

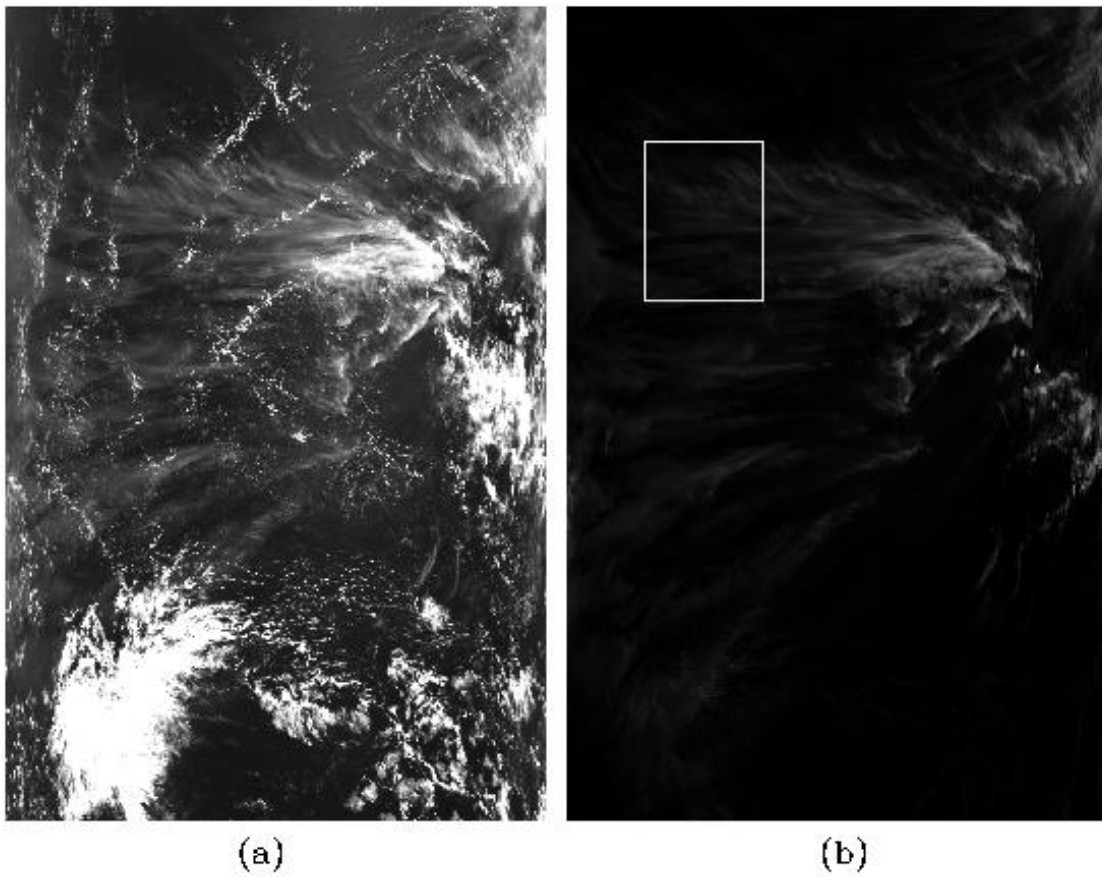


Fig. 7. Terra MODIS level-1b image over the Indian Ocean (July 13, 2003). (a) Visible MODIS image (0.66 μm channel). (b) 1.375 μm channel image corresponding to (a). The white outline indicates the region of optical thickness retrieval.

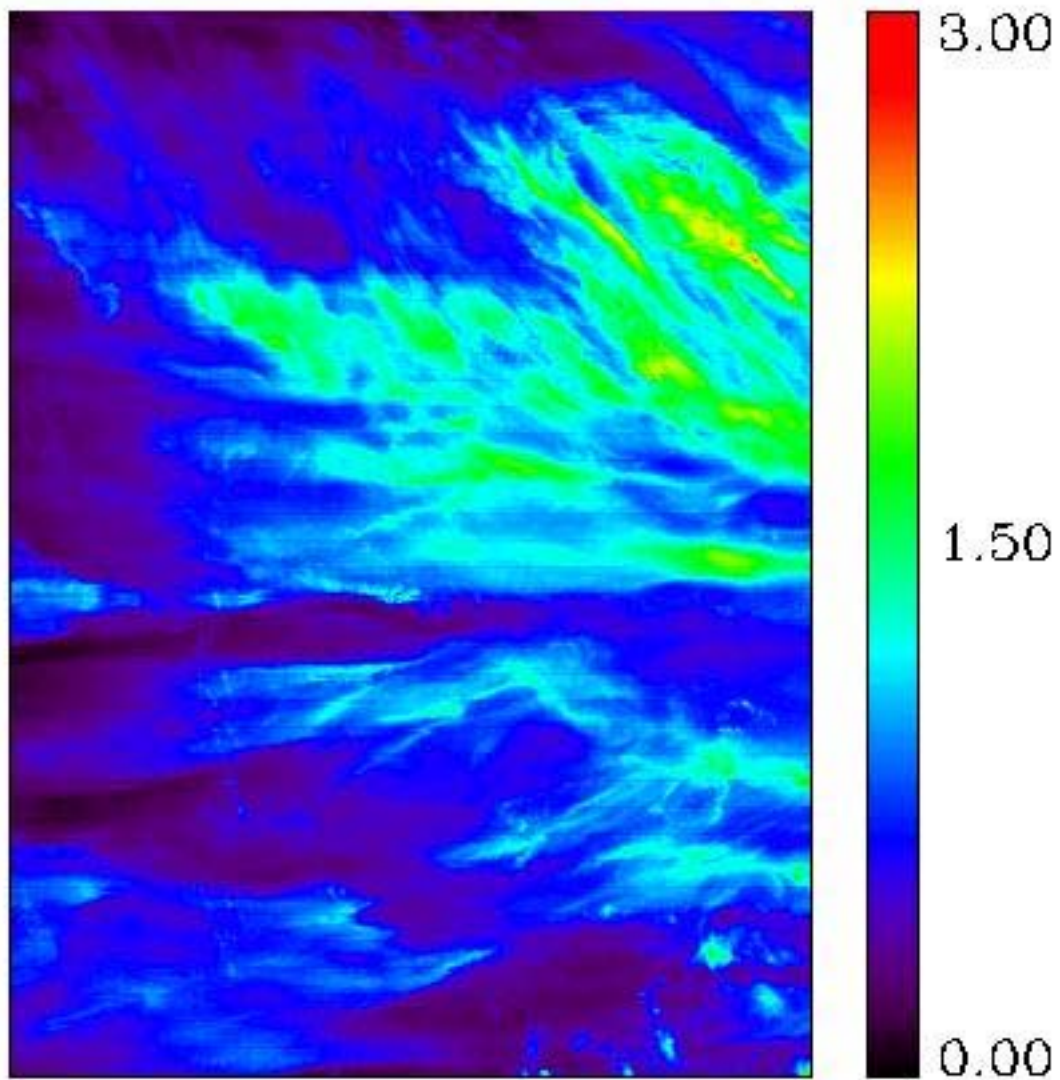


Fig. 8. Retrieved optical thickness of the outlined region in Fig. 7 (b). Note the sensitivity to optically thin cirrus clouds.

Fig. 7 (b) is the $1.375\ \mu\text{m}$ “cirrus” channel image. This image allows for a better view of the spatial extent of cirrus cover in the granule. Clearly, cirrus clouds cover a large portion of this granule, with the possibility of sub-visual cirrus in some regions. The white outline in this image denotes the region of optical thickness retrieval. The selected region has a size of 301×401 pixels. Notice the relatively low reflectance of cirrus clouds within this region, indicating the possible presence of optically thin cirrus.

Fig. 8 shows the retrieved optical thickness of the selected region in Fig. 7 (b). Plotted optical thickness values range from 0.0 to 3.0, as indicated by the bar on the right-hand side. The physical features of the cirrus layer are clearly visible in this image. Also, notice the sensitivity to small optical thickness values in this image (darker shades of blue and purple). These small values indicate the presence of optically thin cirrus.

The second granule used in this study is one over land. Fig. 9 (a) is a visible MODIS image (again using the $0.66\ \mu\text{m}$ wavelength channel) taken over the continent of Africa at 9:25 UTC on January 30, 2003, from the Terra satellite. Surface features are clearly visible in the image (notably in the upper regions of the image). There is also a large presence of convective clouds in the southern portions of the image. On the northern edge of this convection, in the central region of the image, is a small area of thin blow-off cirrus. The retrieval will focus on this region of the granule.

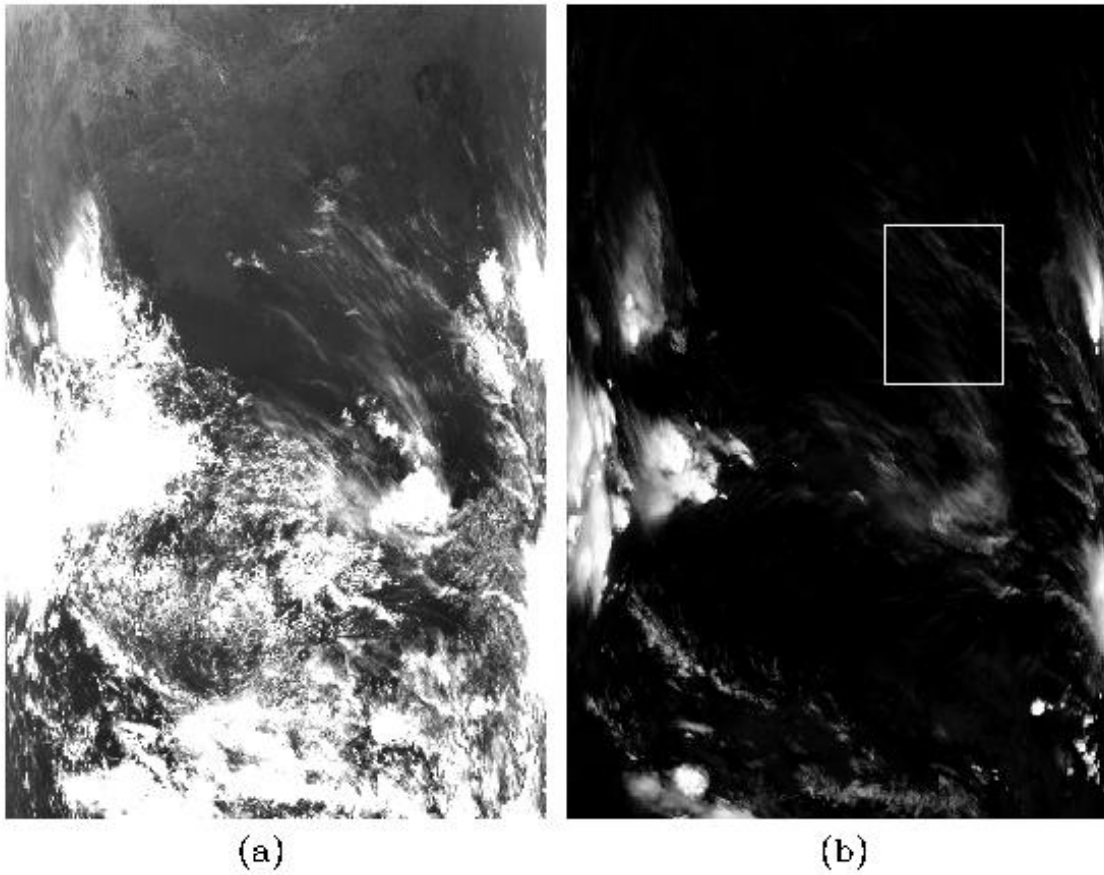


Fig. 9. Terra MODIS level-1b image over Africa (January 30, 2003). (a) Visible MODIS image ($0.66 \mu\text{m}$ channel). Note the surface features evident in the upper region of the image. (b) $1.375 \mu\text{m}$ wavelength image corresponding to (a). The white outline indicates the region of optical thickness retrieval.

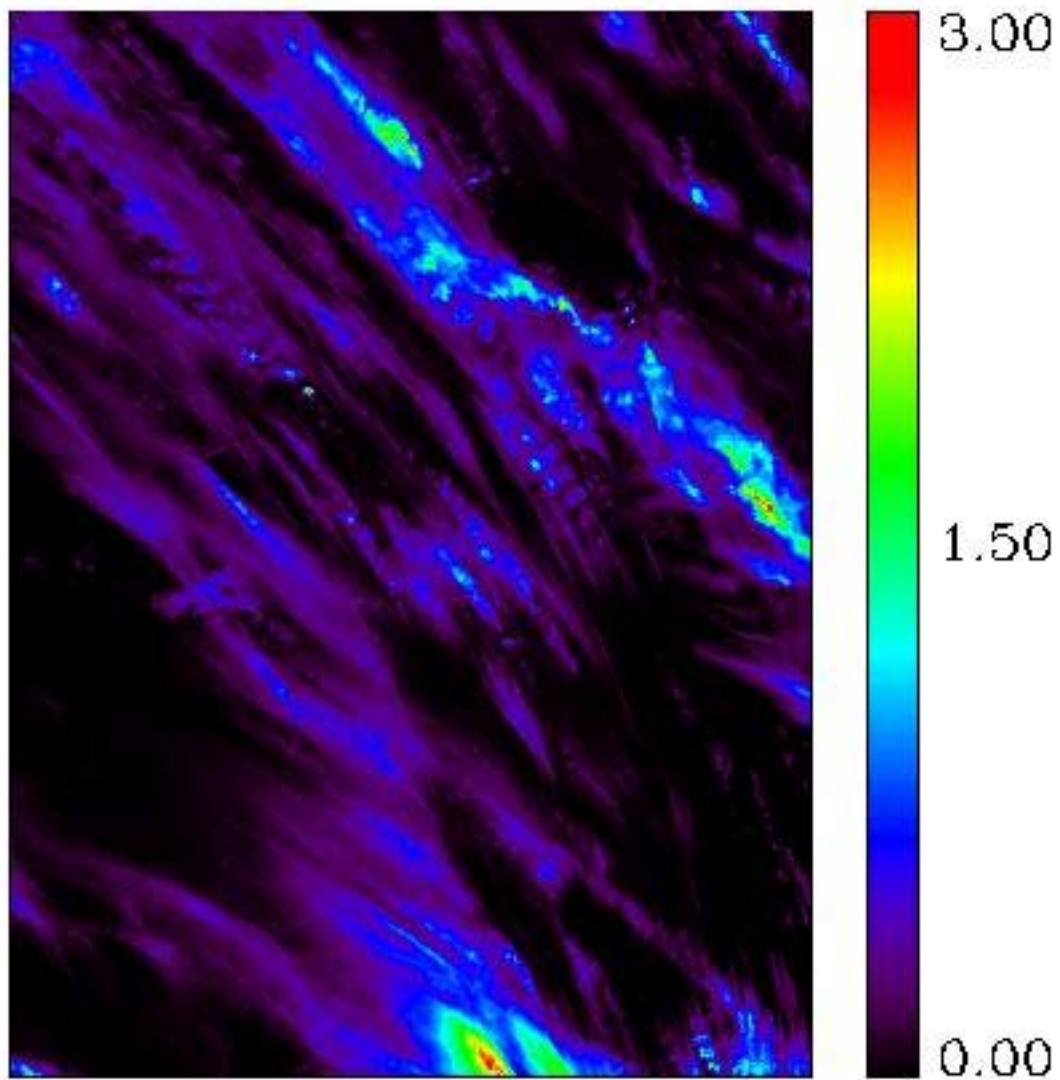


Fig. 10. Retrieved optical thickness of the outlined region in Fig. 9 (b). Note the sensitivity to optically thin cirrus clouds.

Fig. 9 (b) is the corresponding $1.375\ \mu\text{m}$ “cirrus” image. The surface effects and low-level water clouds are now removed. Thick cirrus layers are evident over the regions of convection, while thin blow-off cirrus layers are visible over the center of the image. Again, the white outlined box in this plot indicates the region of optical thickness retrieval. Like the previous granule, this region has a size in pixels of 301×401 .

Fig. 10 shows the retrieved optical thickness of the selected region. Plotted optical thickness values range from 0.0 to 3.0, as indicated by the bar on the right-hand side. Similar to Fig. 8, notice the sensitivity to small values of optical thickness (again, the darker shades of blue and purple). The physical features of the layer are strikingly visible in this image, with the thin, wispy nature of cirrus clouds clearly evident. This image, as well as Fig. 8, illustrates the ability of the algorithm to retrieve the optical thickness of sub-visual cirrus.

As previously stated, our algorithm is complementary to the standard cloud retrieval algorithm [23], [34], which has been implemented as one of the MODIS operational data products. The MODIS operational cloud retrieval algorithm retrieves the optical thickness of all cloud cover observed by MODIS. Using the present algorithm to retrieve the optical thickness of cirrus clouds, it is possible to remove these clouds to obtain the optical thickness of underlying water clouds. This is illustrated in Figs. 11 and 12. Fig. 11 (a) is a $0.66\ \mu\text{m}$ MODIS image over the western equatorial Pacific Ocean on February 6, 2003. Notice the overlay of thin cirrus over low-level convective clouds in the central region of the image. Fig. 11 (b), the corresponding $1.375\ \mu\text{m}$

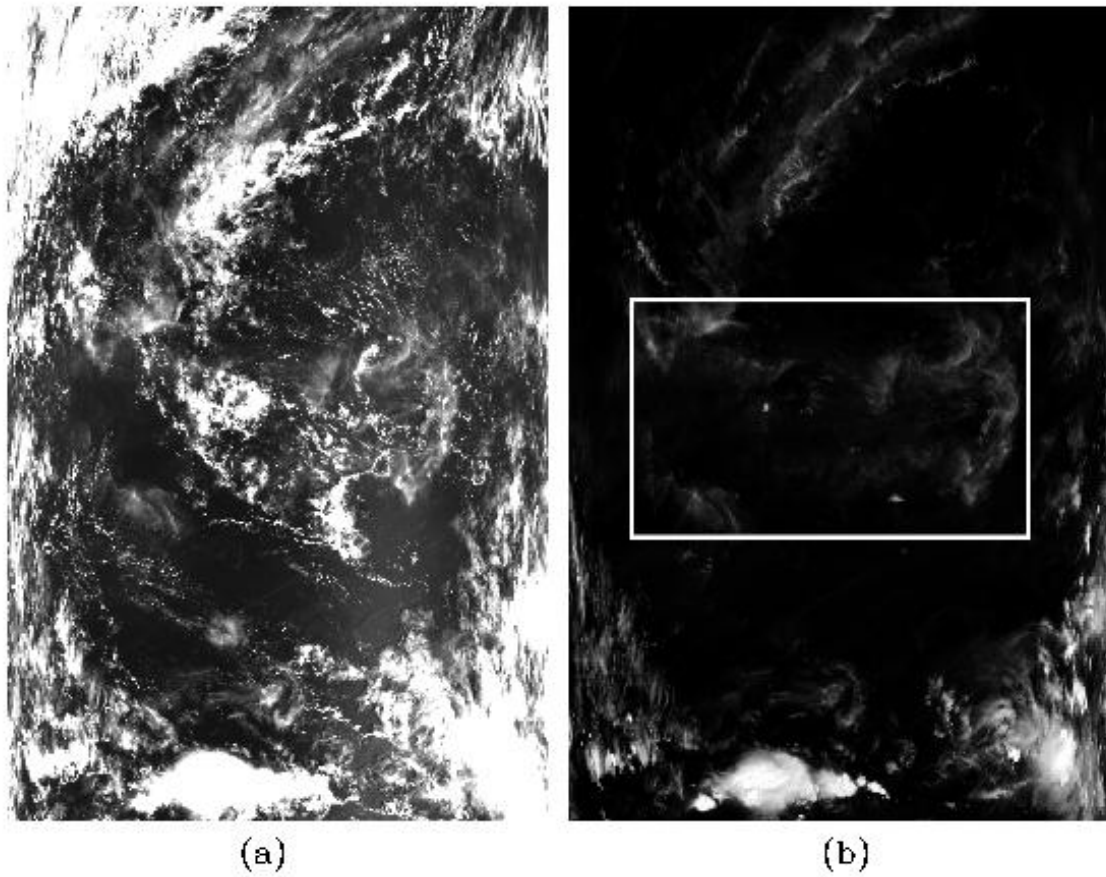


Fig. 11. Terra MODIS level-1b image over the western equatorial Pacific Ocean (February 6, 2003). (a) Visible MODIS image (0.66 μm channel). (b) 1.375 μm wavelength image corresponding to (a). The white outline indicates the region of optical thickness retrieval.

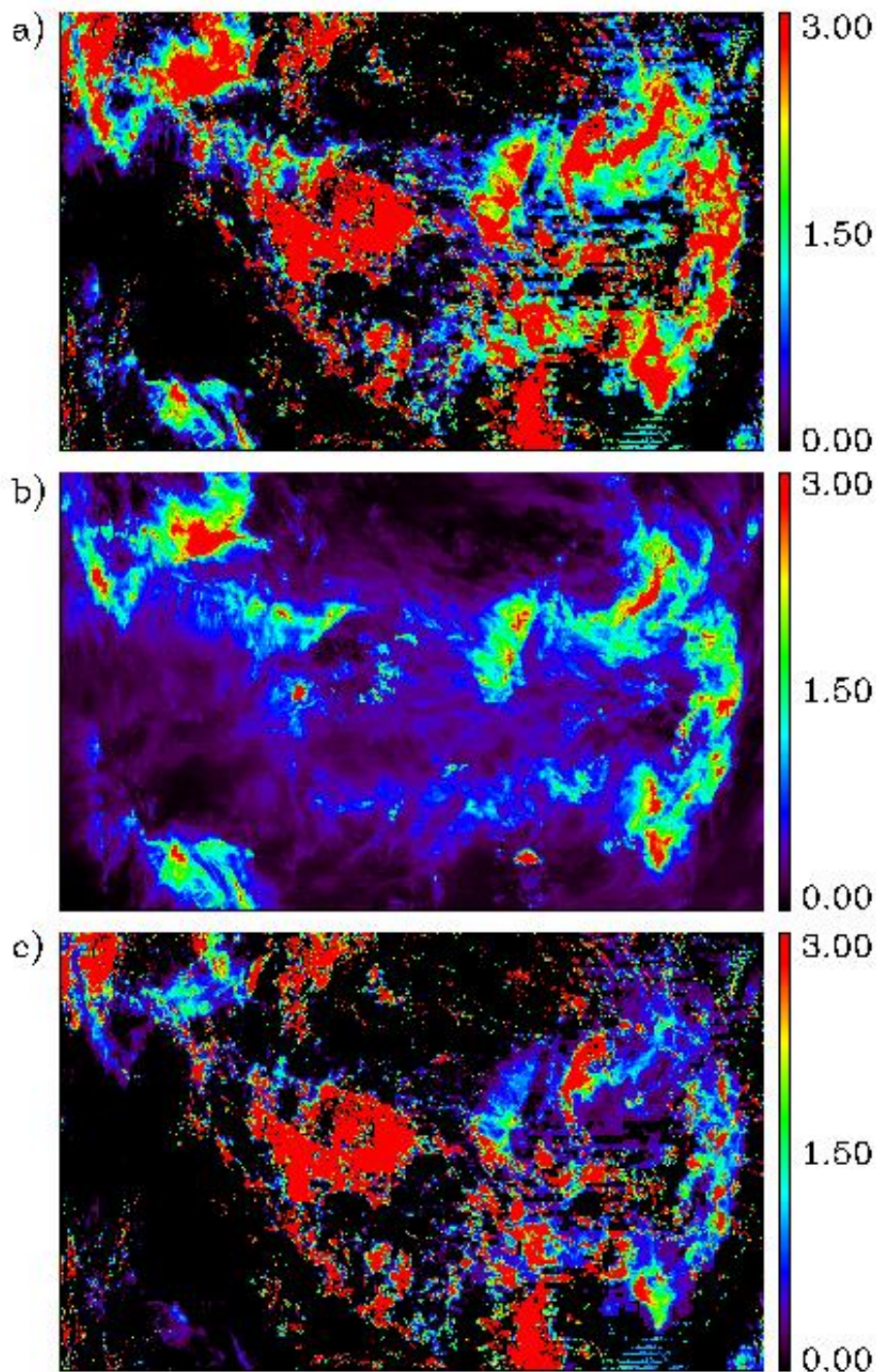


Fig. 12. Retrieved optical thickness images from outlined region in Fig. 11 (b). (a) MODIS operational cloud retrieval algorithm optical thickness image of the outlined region in Fig. 11 (b). (b) Corresponding optical thickness image from the cirrus optical thickness retrieval algorithm. (c) Difference between (a) and (b). Note the absence of high-level cirrus in (c).

image, shows the cirrus cover in more detail. Again, the white outlined box indicates the region of interest.

Figs. 12 (a) and (b) show the retrieved optical thickness from the MODIS operational cloud retrieval algorithm [24], [34] and the present cirrus optical thickness retrieval algorithm, respectively. Similar to Fig. 11 (a), the high-level cirrus overlay is clearly visible in Fig. 12 (a). Fig. 12 (b) can now be subtracted from Fig. 12 (a) to obtain the low-level water cloud optical depth image. In Fig. 12 (c), high-level cirrus has been removed, revealing the optical thickness of the underlying water clouds.

3.3 Discussion/Summary

In this study, an algorithm was developed to retrieve the optical thickness of tropical cirrus clouds using cirrus visible reflectance derived from MODIS bands 1 and 26, which are publicly available. An optical properties database consisting of the mean scattering and absorption properties of several different ice crystal habits for various experimentally measured size distributions using previously calculated scattering and optical properties data [49] was first constructed. The Discrete Ordinates Radiative Transfer (DISORT) code was then used to establish a correlation between tropical cirrus reflectance and cloud optical thickness. Data from the optical properties database were used for these DISORT calculations. All atmospheric and surface effects were assumed to be negligible in these calculations. Reflectance of $0.66 \mu\text{m}$ radiation by cirrus clouds is sensitive only to cirrus optical thickness. It is therefore possible to retrieve the optical thickness of tropical cirrus clouds, given the satellite viewing geometry and the $0.66 \mu\text{m}$

reflectance values. An optical thickness look-up library was then created consisting of data from a “representative” tropical cirrus size distribution, in this case the median of the nine CEPEX size distributions.

An algorithm was then developed to retrieve the optical thickness of tropical cirrus using MODIS level-1b radiance data. Atmospheric and surface effects are removed from the data using the cirrus reflectance retrieval algorithm. The optical thickness retrieval algorithm was then integrated into the cirrus reflectance algorithm. It should be noted that the present algorithm is not an operational algorithm. It has been developed to compliment the aforementioned MODIS cloud retrieval algorithm (currently implemented as one of the MODIS operational data products) for the case of cirrus clouds. This approach is especially effective for isolated cirrus clouds, but is also effective for the case of cirrus over water clouds, or cloud overlap. This is illustrated using calibrated reflectance data from the MODIS instrument on board the Terra satellite.

4. SURVEY OF TROPICAL CIRRUS OPTICAL THICKNESS USING MODIS LEVEL-3 DATA

In order to understand the effects of cirrus clouds on the earth's radiative processes and climate system, a good knowledge of the nature, spatial extent, location, and frequency of occurrence of such clouds is needed. With the development of MODIS and the subsequent inclusion of the 1.375 μm "cirrus detection" channel, an unprecedented global view of cirrus cloud cover is now possible. As an extension of Section 3, a preliminary survey of the optical thickness fields of tropical cirrus clouds has been undertaken. This includes the extent of cirrus cover in the tropics, as well as frequency of occurrence.

4.1 Methodology

The general methodology for the preliminary study of tropical cirrus cloud optical thickness is fairly straightforward. Cloud optical thickness is first retrieved from MODIS level-3 daily gridded atmospheric data, which are available to the public. These data contain daily mean cirrus reflectance values, relative azimuth angles, and solar and viewing zenith angles. For the retrieval, the tropical cirrus optical thickness retrieval algorithm from Section 3 is modified to accept level-3 data as input. The daily mean tropical cirrus optical thickness is retrieved for each calendar day. Analyses of tropical cirrus cover can then be completed.

4.2 Retrieval

4.2.1 *MODIS Level-3 Daily Gridded Data*

MODIS level-3 daily gridded atmospheric data are a global product. They contain over 500 statistically averaged atmospheric parameters at a 1 degree by 1 degree spatial resolution. All level-3 atmospheric parameters are derived from four level-2 MODIS atmospheric products (Aerosol, Water Vapor, Cloud, and Atmosphere Profile). These parameters are averaged over a 1 degree by 1 degree grid spacing for a 24-hour time period (0000 to 2400 GMT), producing a daily 360 by 180 pixel grid as output. They include actual atmospheric values, as well as standard deviations, quality assurance weighted means and other statistically derived quantities for each parameter. Of these parameters, isolated cirrus reflectance, derived from the operational algorithm of Gao et al. [14], and the corresponding solar/satellite view geometries are of importance to the present study. Level-3 daily gridded atmospheric data, from February 2000 to the present, are publicly available through the NASA Distributed Active Archive Center (DAAC). These data will be used as input to a modified tropical cirrus optical thickness retrieval algorithm.

4.2.2 *Tropical Cirrus Optical Thickness Retrieval Algorithm*

The retrieval algorithm described in Section 3 is used in the present study to retrieve the optical thickness of tropical cirrus clouds using MODIS level-3 daily gridded data. This algorithm, however, is written to operate on MODIS level-1b data. A modified version of the algorithm is therefore necessary for the retrieval described here.

Level-1b data is regional in scope and has a pixel resolution of 1354×2030 (1 km by 1 km grid). As described above, MODIS level-3 data is global in scale with a pixel resolution of 360×180 . The algorithm's input pixel resolution is reduced to the level-3 resolution. In addition, level-1b data contain raw reflectance values, and therefore the isolated cirrus reflectance must be derived in the retrieval algorithm using the method of Gao et al. [14]. Level-3 data, however, contain operationally derived isolated cirrus reflectance. Therefore, the cirrus reflectance algorithm is removed from the optical thickness retrieval code. Derived cirrus reflectance, as well as the solar/sensor zenith angles and relative azimuth angles, are directly input into the retrieval code. Optical thickness retrieval then follows the same method described in Section 3.

4.3 Preliminary Results

For the present study, the retrieval code has been run on fourteen consecutive months of MODIS level-3 data. These data are from the Terra satellite, and cover the months from September 2001 to October 2002. Only data between 30° N and 30° S are considered. Derived isolated cirrus reflectance values and solar/satellite view geometry data have been extracted and stored in daily data files. These files serve as input for the retrieval code. It should be noted that, since only just over a year of data is used, the results discussed here are not statistically sound. However, they do provide a glimpse of the many studies that can be performed using this method.

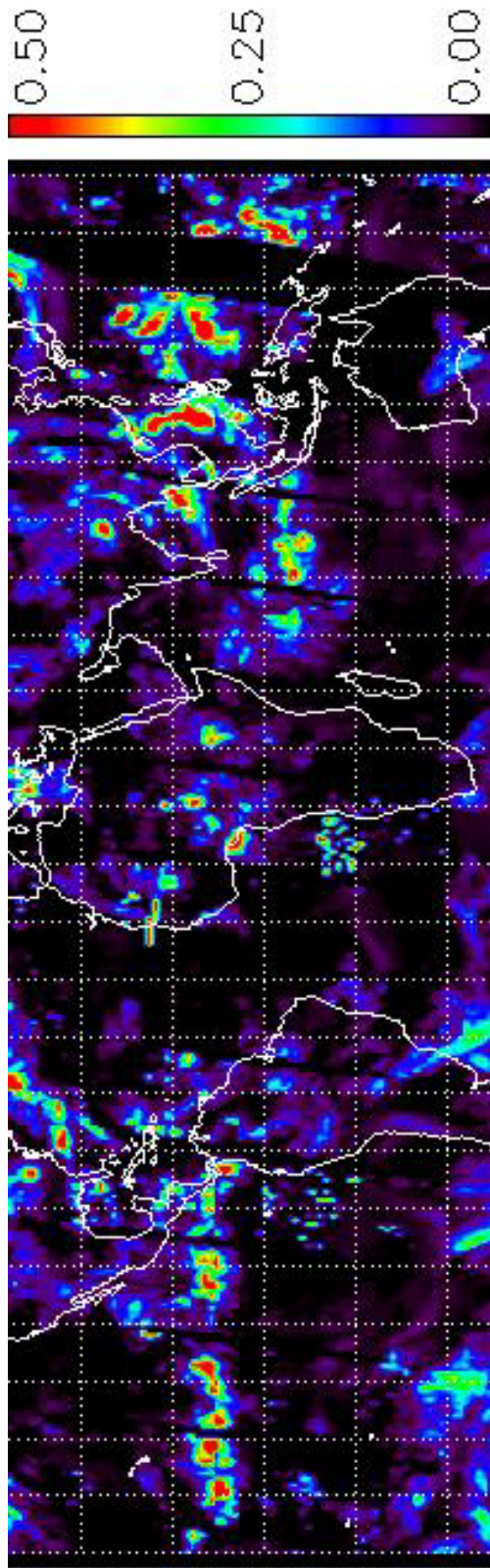


Fig. 13. MODIS level-3 derived isolated cirrus reflectance from Terra satellite on July 27, 2002.

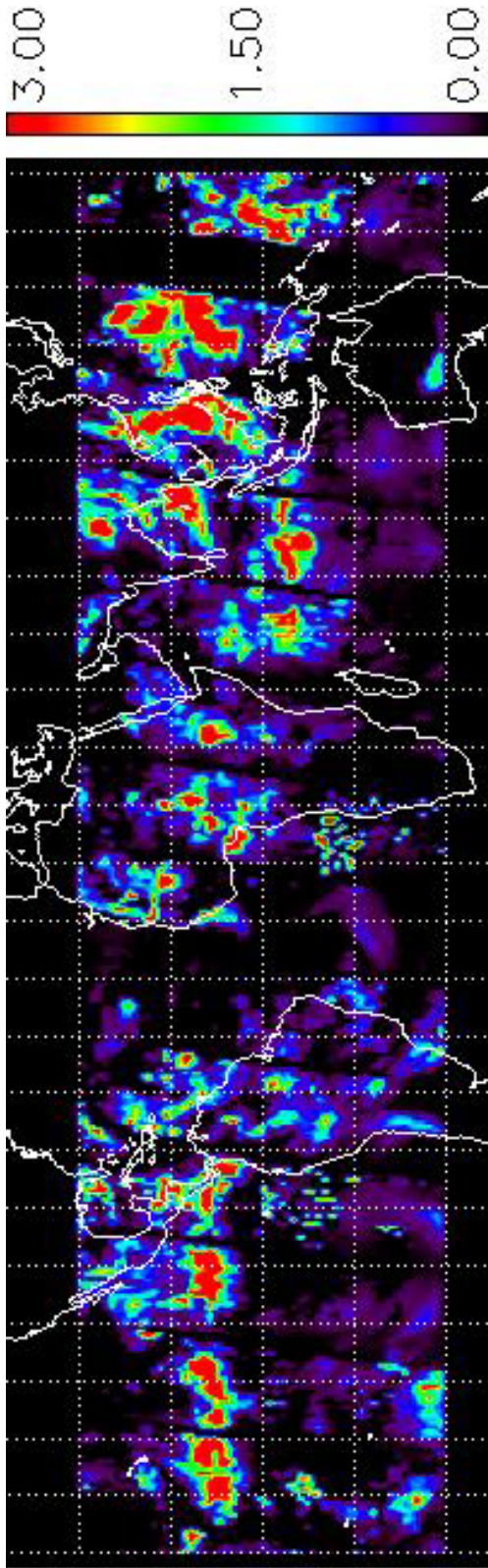


Fig. 14. Tropical cirrus optical thickness derived from MODIS level-3 cirrus reflectance corresponding to Fig. 13.

Fig. 13 shows a sample MODIS level-3 mean cirrus reflectance image from the Terra satellite for July 27, 2002. Cirrus reflectance values are scaled between 0.0 and 0.5, as indicated by the bar on the right-hand side. Most of the cirrus in this image appears to be due to convective storms along the Intertropical Convergence Zone (ITCZ), which is visible in a line of convection just north of the equator. High reflectance values in this image indicate relatively thick cirrus clouds. Note the concentration of cirrus over the western equatorial Pacific Ocean. This region experiences relatively frequent convection, especially during the summer monsoon.

Fig. 14 shows the derived cirrus optical thickness plot corresponding to the image in Fig. 13. Optical thickness values are scaled between 0.0 and 3.0, as indicated by the bar on the right-hand side. This image appears very similar to Fig. 13, as is expected. Again, the ITCZ is clearly visible just north of the equator. Note that the areas of large optical thickness in this figure correspond to the areas of high cirrus reflectance in Fig. 13.

Fig. 15 shows the total number of days with cirrus optical thickness greater than zero for the entire 14-month period between September 2001 and October 2002. This image is scaled from 0 to 400 days, as indicated by the bar on the right-hand side. The ITCZ appears as a thin band just north of the equator, except over Indonesia, where it widens significantly. Note the relatively high frequency of cirrus cover over mountainous areas such as the Andes in South America, the Himalayas in southern Asia, and to a lesser extent the Sierra Madre Occidental and Sierra Madre Del Sur in the western portions of Mexico. These patterns can be attributed to large-scale orographical lifting in these

regions. Also note the relatively high frequency of cirrus over the western equatorial Pacific Ocean (particularly over Indonesia). This can be attributed to the frequent convection experienced over this region.

Fig. 16 shows the number of days with cirrus optical thickness greater than zero during the winter months of December 2001, and January and February 2002. This image is scaled from 0 to 90 days, as indicated by the bar on the right-hand side. Note that regions of highest cirrus frequency are located over large landmasses (e.g., South America, southern Africa) and the islands of Indonesia. As expected, these regions are also slightly south of the equator, due to the southern hemisphere summer and subsequent southward movement of the ITCZ. Also, the aforementioned mountainous areas are evident in this image.

Fig. 17 shows the number of days with cirrus optical thickness greater than zero during the summer months of June, July, and August 2002. This image is scaled between 0 and 90 days, as indicated by the bar on the right-hand side. A more continuous and defined ITCZ is clearly evident in this image. Note the northward movement of the regions of highest cirrus frequency, especially those over large landmasses, which is due to the northern hemisphere summer. Also, note the significantly large area of high frequency of cirrus occurrence over southern Asia, undoubtedly due to the summer monsoons in this region.

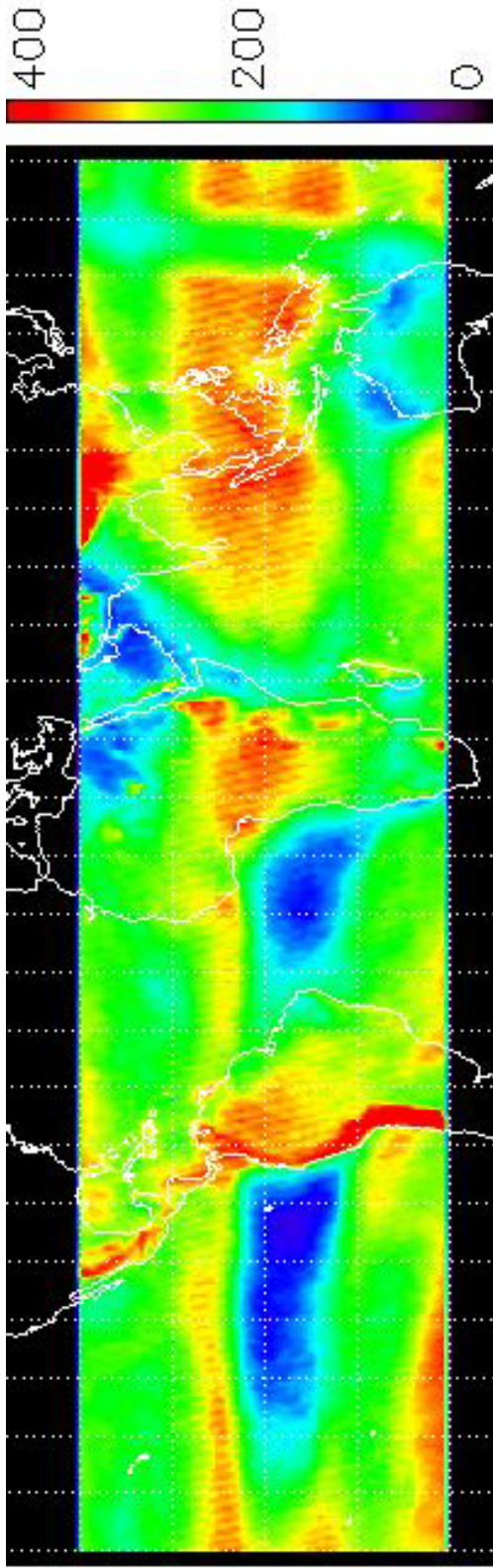


Fig. 15. Total number of days between September 2001 and October 2002 with cirrus optical thickness greater than zero.

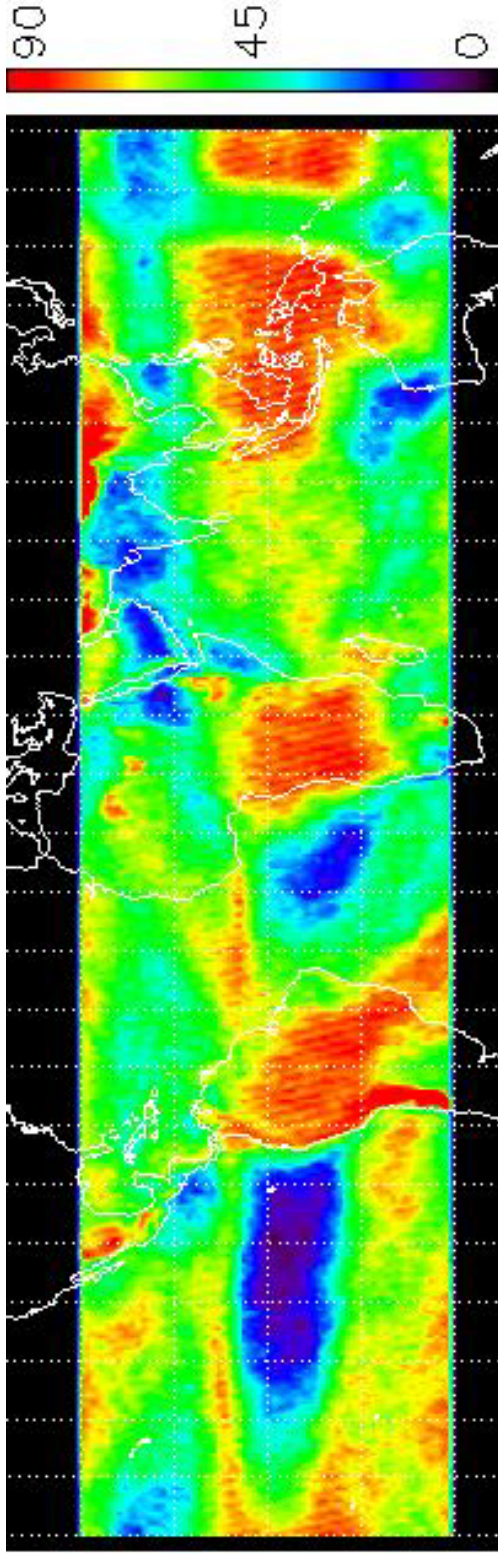


Fig. 16. Number of days during the winter months of December, January, and February with cirrus optical thickness greater than zero.

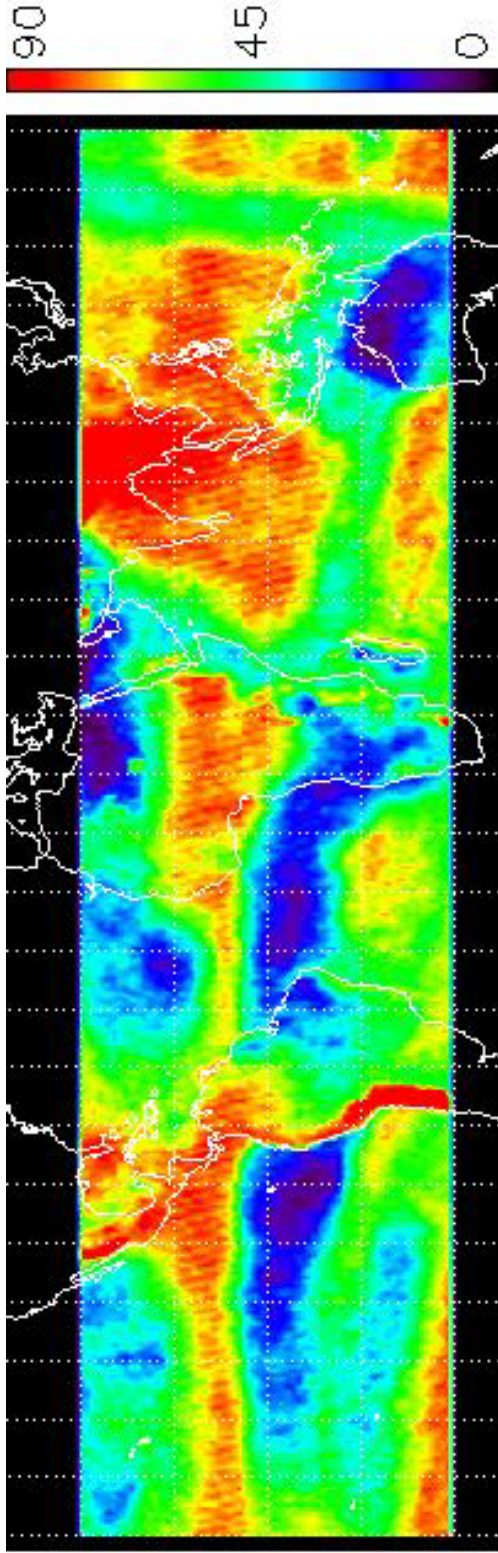


Fig. 17. Number of days during the summer months of June, July, and August with cirrus optical thickness greater than zero.

4.4 Discussion/Summary

The tropical cirrus optical thickness algorithm discussed in Section 3, when applied to MODIS level-3 daily gridded data, can provide an impressive view of cirrus cover in the tropics. While the preliminary results discussed here should not be considered a sound statistical study, they do offer a glimpse of possible future endeavors using MODIS level-3 daily gridded data with the optical thickness retrieval algorithm. A more in depth analysis, taking into consideration meteorological processes and geographical effects, can provide a more accurate study of tropical cirrus optical thickness fields.

5. CIRRUS OPTICAL THICKNESS AND EFFECTIVE SIZE FROM AVIRIS DATA*

5.1 Background

5.1.1 *The AVIRIS Instrument*

AVIRIS (Airborne Visible Infrared Imaging Spectrometer) is a hyperspectral imaging instrument designed and built at the Jet Propulsion Laboratory [40], [16]. The imaging data acquired with AVIRIS have been used in a variety of research and applications, including geology, agriculture, forestry, coastal and inland water studies, environment hazards assessment, and urban studies [6]. AVIRIS is now an operational instrument with reliable radiometric and spectral calibrations. It is equipped to view 224 narrow channels with widths of approximately 10 nm, covering the contiguous solar spectral region between 0.4 and 2.5 μm . AVIRIS typically acquires images with a pixel size of 20 m from a NASA ER-2 aircraft at an altitude of 20 km. The swath width on the ground is approximately 12 km. AVIRIS can also acquire images from a low-altitude aircraft at spatial resolutions of 1 to 4 m with reduced swath widths.

5.1.2 *Cirrus Detections*

Previously, it was reported [11], [12] that narrow channels near the centers of the 1.38 and 1.88 μm strong water vapor absorption bands are very effective in detecting

*This work has been submitted to the IEEE for possible publication.

thin cirrus clouds based on the analysis of AVIRIS data collected in the late 1980s and early 1990s. The mechanisms for cirrus detection are relatively simple. In the absence of cirrus clouds, these narrow channels receive little solar radiance scattered by the surface and low-level water clouds because of the strong absorption of solar radiation by atmospheric water vapor located above them. When high-level cirrus clouds are present, these channels receive solar radiances scattered by cirrus clouds that contrast well on the dark background.

During the mid-1990s, a major upgrade to the AVIRIS instrument was made. The signal to noise ratios of AVIRIS data improved significantly. Here, the newer AVIRIS data sets are preferred to demonstrate again the capability of cirrus detections with narrow channels near 1.38 and 1.88 μm . Fig. 18 (a) shows a true color AVIRIS image (red: 0.66 μm ; green: 0.55 μm ; blue: 0.47 μm) acquired over Bowie, Maryland, near a latitude of approximately 38.97°N and a longitude of approximately 76.74°W on July 7, 1996. Surface features are seen through the partially transparent thin cirrus clouds. Figs. 18 (b) and 18 (c) show the 1.38- μm image and the 1.88- μm image, respectively. Both channels allow for the detection of thin cirrus clouds.

5.1.3 Cirrus Reflectance Properties

In order to illustrate the reflectance properties of cirrus clouds, Fig. 19 shows an “apparent reflectance” spectrum measured over an area covered by cirrus clouds above Monterey Bay, California, on September 4, 1992. Omitting for convenience the

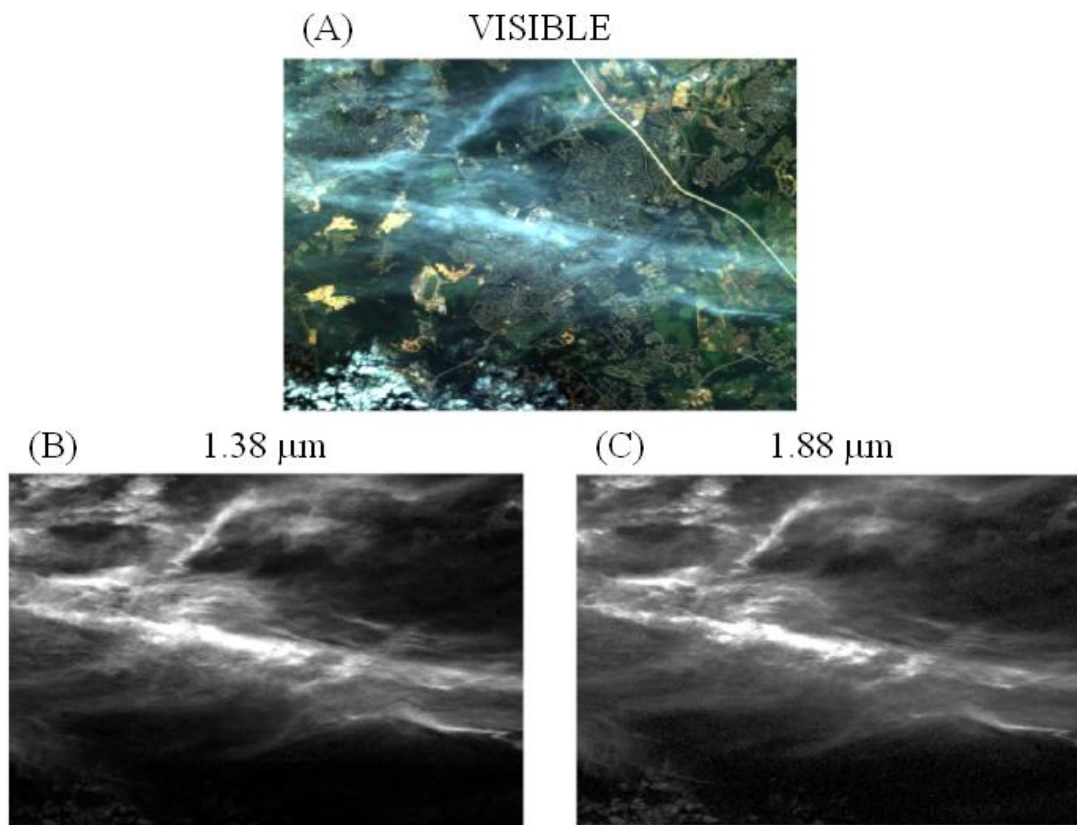


Fig. 18. Sample AVIRIS images. (a) A true color AVIRIS image (red: 0.66 μm ; green: 0.55 μm ; blue: 0.47 μm), (b) the 1.38- μm channel image, and (c) the 1.88- μm channel image processed from the AVIRIS data acquired over Bowie in Maryland near a latitude of approximately 38.97°N and a longitude of about 76.74°W on July 7, 1996. Surface features are seen in (a), and thin cirrus clouds are seen in (b) and (c).

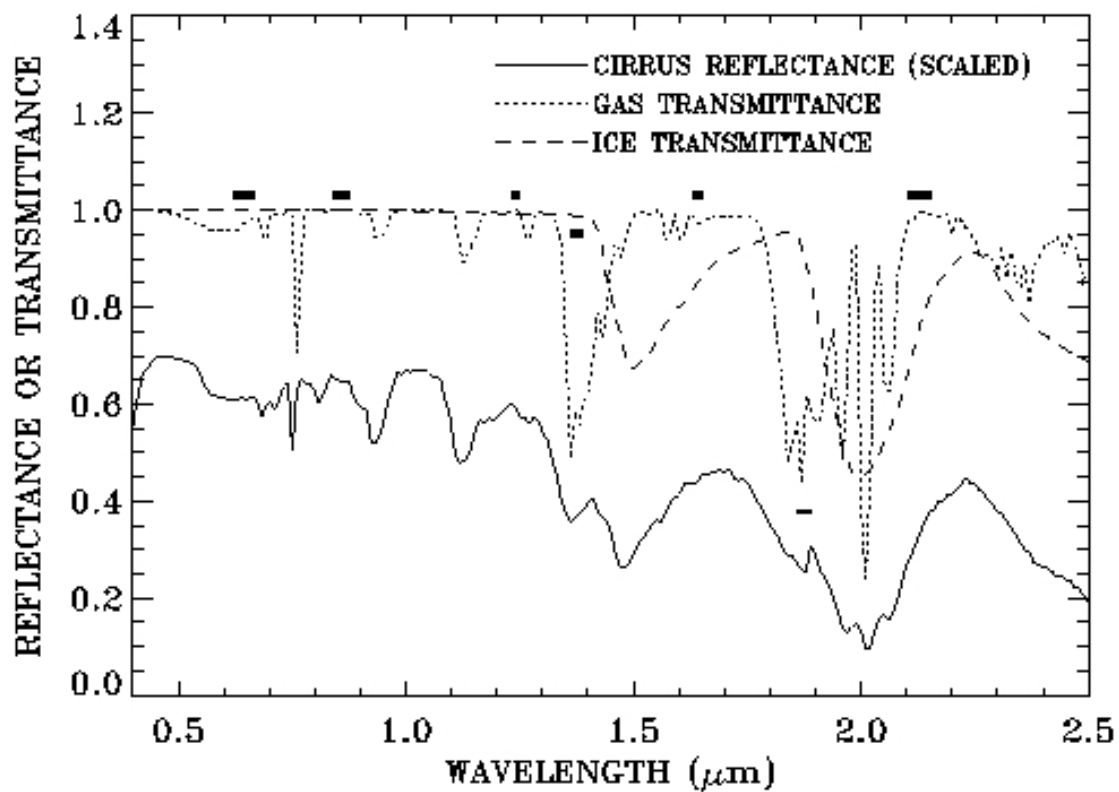


Fig. 19. A cirrus reflectance spectrum measured by AVIRIS. Taken over an area above Monterey Bay, California, on September 4, 1992. Also an atmospheric gas transmittance spectrum and an ice transmittance spectrum.

wavelength (λ) and cosine-solar-zenith-angle (m_0) dependencies, the “apparent reflectance” at the aircraft or satellite is denoted as

$$r^* = p L / (m_0 E_0), \quad (17)$$

where L is the radiance measured by the satellite and E_0 is the extra-terrestrial solar flux. The cirrus spectrum was scaled to 0.7 near $0.5 \mu\text{m}$ in order to avoid the overlapping of this curve with the other two curves in the plot. The absorption features of the atmospheric oxygen band centered near $0.76 \mu\text{m}$, water vapor bands near 0.94 , 1.13 , 1.38 , and $1.88 \mu\text{m}$, and a carbon dioxide band near $2.06 \mu\text{m}$ are seen in this spectrum. These features are the result of absorption by atmospheric gases located above and within cirrus clouds. The solar radiation transmitted through cirrus clouds in the downward path is mostly absorbed by atmospheric gases below cirrus and by liquid water in the ocean. The ice absorption bands centered near $1.5 \mu\text{m}$ and $2.0 \mu\text{m}$ are also seen. These bands are resulted from absorption by ice particles within cirrus clouds. In order to help identify various absorption features contained in the cirrus spectrum, an atmospheric gas transmittance spectrum and an ice transmittance spectrum (0.007 cm thick) are also shown. Weak ice absorption occurs near 1.24 and $1.38 \mu\text{m}$. The effects at both wavelengths are expected to be about the same, since the imaginary parts of the ice refractive index [25] are comparable.

The positions and widths of five MODIS visible and near-IR atmospheric window channels used in the operational retrievals of MODIS cloud optical properties [24], [34] and the $1.375\text{-}\mu\text{m}$ cirrus detecting channel are shown in thick horizontal bars above the

transmittance spectra in Fig. 19. A narrow channel centered near $1.88 \mu\text{m}$ with a width of 30 nm , which is absent in any of the current or near-future meteorological satellite sensors for cirrus detections, is also illustrated with a thinner horizontal bar in the lower right portion of the plot. From the ice transmittance spectrum and cirrus reflectance spectrum, it is seen that the ice absorption effect over the bandpass of the $1.375 \mu\text{m}$ channel is weak, while the absorption effect over the bandpass of the $1.88 \mu\text{m}$ channel is stronger. This difference allows, in principle, the simultaneous retrieval of optical depths and ice particle size distributions using both channels with little contamination from the surface or lower level water clouds (see Figs. 18 (b) and 18 (c)). Because the two channels are located within water vapor absorption regions (see the cirrus reflectance spectrum and gas transmittance spectrum), the water vapor absorption effects must be properly modeled and removed before the two channels can be used for the quantitative retrieval of cirrus optical properties.

5.2 Method

An empirical technique for estimating water vapor transmittances was previously described in detail [13]. Over water surfaces, the scatter plot of the $1.375 \mu\text{m}$ channel apparent reflectance values ($r_{1.375}^*$) versus the $1.24 \mu\text{m}$ channel apparent reflectance values ($r_{1.24}^*$) is made. The slope of an empirically established line is estimated [13], and this slope is considered to be the water vapor transmittance ($T_{1.375}$) for the $1.375 \mu\text{m}$ channel. Over land surfaces, the water vapor transmittance for the $1.375 \mu\text{m}$ channel is similarly derived, except that the $0.66 \mu\text{m}$ channel is used in place of the $1.24 \mu\text{m}$

channel . Because the ice particle absorption effect near 1.375 μm is weak, the intrinsic cirrus reflectance for the 1.375 μm channel, $r_{1.375}$, is approximately equal to the ratio of $r_{1.375}^* / T_{1.375}$. This intrinsic reflectance is related to the cirrus optical depth [31].

For the 1.88 μm channel, both the atmospheric water vapor absorption effect and the ice particle absorption effect are significant (see Fig. 19). The 1.88 μm channel water vapor transmittance, $T_{1.88}$, is predicted using the estimated 1.375 μm channel water vapor transmittance, $T_{1.375}$, and a line-by-line atmospheric transmittance code. The HITRAN2000 line database [37] is used in the line-by-line calculations. The intrinsic cirrus reflectance for the 1.88 μm channel, $r_{1.88}$, is equal to the ratio of $r_{1.88}^* / T_{1.88}$. This intrinsic reflectance is related to both the cirrus optical depth and the ice particle size distributions.

After obtaining the intrinsic cirrus reflectances for both the 1.375 and 1.88 μm channels, the retrieval of cirrus optical depth and ice particle size can be made using the well established Nakajima and King [32] approach. In order to do so, look-up tables for each sun/satellite viewing geometry (i.e., relative azimuth angle, as well as solar and viewing zenith angles) must first be generated. Each look-up table should include the 1.38 and 1.88 μm reflectance values, along with the corresponding optical thickness and effective diameter values. The Discrete Ordinates Radiative Transfer (DISORT) code [39] is used for all radiance calculations under the assumption of isolated cirrus clouds with no atmosphere above and below the clouds. This assumption is justified because the Rayleigh scattering effects for wavelengths greater than about 1 μm are negligible.

Cirrus scattering properties (used as input for DISORT) are averaged from the results of Yang et al. [49].

Fig. 20 shows the single-scattering phase functions for both the 1.38 and 1.88 μm channels averaged from Yang [49]. The eight mid-latitude size distributions used in the DISORT-generated look-up tables are shown in this plot, with effective diameters ranging from 9.2 to 146.1 μm . The assumed habit percentages are shown in the 1.38 μm plot. For effective diameters less than 70 μm , a habit percentage of 50% bullet rosettes, 25% plates, and 25% columns is assumed. For diameters greater than 70 μm , a composition of 30% rough aggregates, 30% bullet rosettes, 20% columns, and 20% plates is assumed [1].

Fig. 21 (a) shows a sample look-up table generated for one case study of AVIRIS data (236.41° relative azimuth, 44.34° solar zenith, and nadir viewing zenith). Lines of constant ice crystal effective diameter and cirrus optical thickness are labeled. Note the sensitivity of the 1.38 μm wavelength to optical thickness, and the sensitivity of the 1.88 μm wavelength to effective diameter. For a given pair of intrinsic reflectance values of the 1.38 and 1.88 μm channels, simultaneous retrievals of the optical thickness and ice crystal size distribution can, in principle, be made using the simulated lookup table and a simple table-searching procedure. Fig. 21 (b) shows a close-up of Fig. 21 (a), with AVIRIS data superposed. The data used in this image are from the natural cirrus image (Scene 3) described below.

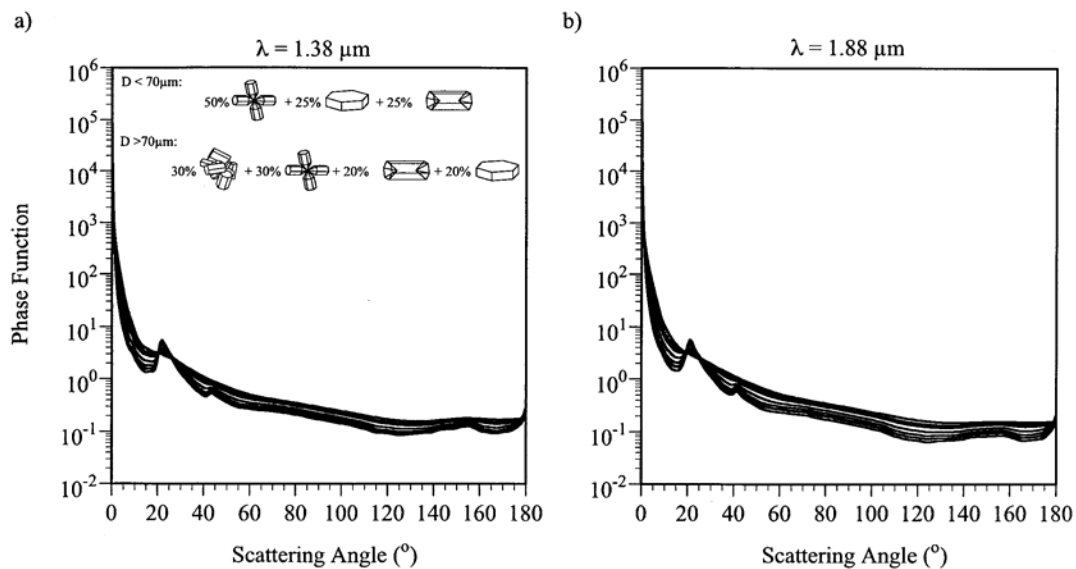


Fig. 20. Mid-latitude cirrus phase functions. (a) Scattering phase function plot for the $1.38 \mu\text{m}$ channel. (b) Scattering phase function plot for the $1.88 \mu\text{m}$ channel. The habit percentage used in this study is shown in the $1.38 \mu\text{m}$ plot.

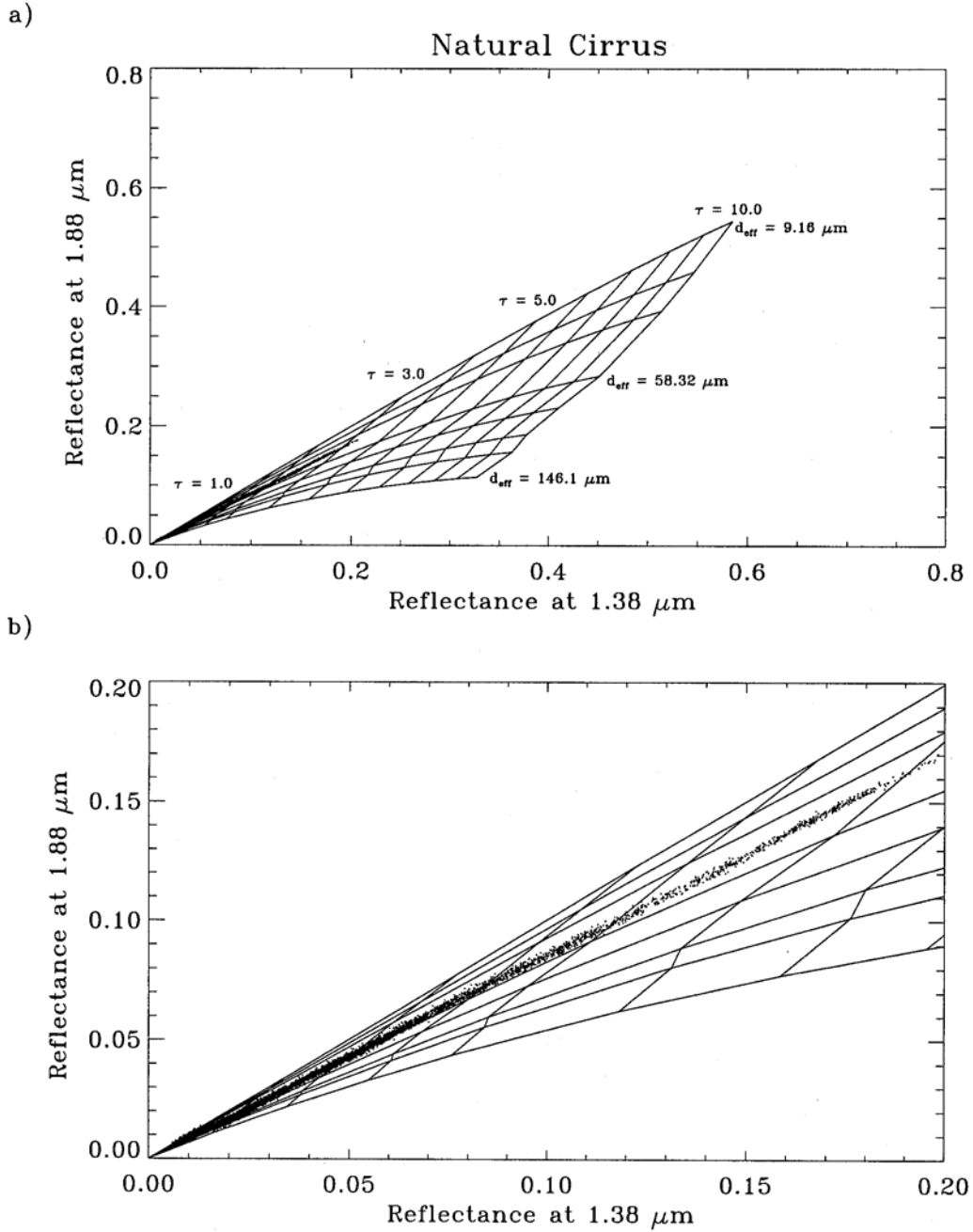


Fig. 21. Sample look-up table for AVIRIS retrieval. (a) Sample look-up table for the natural cirrus shown in Scene 3 (236.41° relative azimuth, 44.34° solar zenith, and nadir viewing zenith). (b) Close-up of (a) with Scene 3 AVIRIS data superposed.

5.3 Preliminary Results

The method described in Section III has been applied to three sets of AVIRIS data, one containing aircraft-induced contrail cirrus (Scene 1) and two containing natural cirrus (Scenes 2 and 3). Scenes 1 and 2 were taken over the coastal areas of New Jersey on July 12, 1998 during the Long-term Ecosystem Observatory in 15 meters (LEO-15) experiment [41]. LEO-15 was primarily designed for the study of shallow coastal waters. Scene 3 was taken over Monterey Bay, California on September 4, 1992. The cirrus-contaminated AVIRIS data is used for the research on simultaneous retrievals of optical depths and ice particle size distributions. The preliminary retrieval results from the three AVIRIS data sets are described below.

5.3.1 *Contrail Cirrus (Scene 1)*

Fig. 22 (a) shows the 1.24 μm channel image for the scene containing contrail cirrus. The image covers an area of about 12 km by 10 km. It has 614 pixels from left to right and 512 pixels from top to bottom. Most of the scene is covered by water, and only a small fraction of the scene is covered by land. The center of the image is located at approximately 39.47°N and 76.25°W. Small white dots are seen throughout the image. These dots represent the wakes of boats in the water. The contrail itself is very thin (very small reflectance), and stretches from left to right across the image. Fig. 22 (b) is the 1.38 μm channel image. The contrail cirrus is clearly seen. The boat wakes disappear in this image due to strong absorption by water vapor below the contrail cirrus. Fig. 22 (c) shows the 1.88 μm image. It is almost identical to the image in Fig. 22 (b)

with the exception that the reflectance values are smaller than those of the 1.38 μm channel.

Fig. 23 shows the scatter plot of the 1.38 μm channel apparent reflectance values ($r_{1.375}^*$) versus the 1.24 μm channel apparent reflectance values ($r_{1.24}^*$) for the scene in Fig. 22. The lower portion of the plot contains land pixels with larger 1.24 μm reflectance values. Pixels covered by the contrail cirrus over the dark water surfaces are clustered around a steep line at left, which has a slope of about 0.8. This slope is the estimate of the water vapor transmittance ($T_{1.375}$) for the 1.375 μm channel. The derivations of the intrinsic cirrus reflectance values for the 1.375 μm channel ($r_{1.375}$) and the 1.88 μm channel ($r_{1.88}$) are subsequently made using the techniques outlined in Section 5.2. In order to improve the signal to noise ratios of the intrinsic cirrus reflectances ($r_{1.375}$ and $r_{1.88}$), a spatial averaging of the data is performed. The resulting data set has only 76 x 64 pixels.

During the practical retrieval process, the retrieval code has been written for each set of AVIRIS image data using the computed scene-specific look-up table. The look-up table resolution is doubled four times (from 8 effective diameters and 17 optical depths to 113 effective diameters and 273 optical depths) using linear averaging. A simple averaging of the optical thickness and effective diameters of the four nearest look-up table points to each data pixel (effectively a data “box”) is performed.

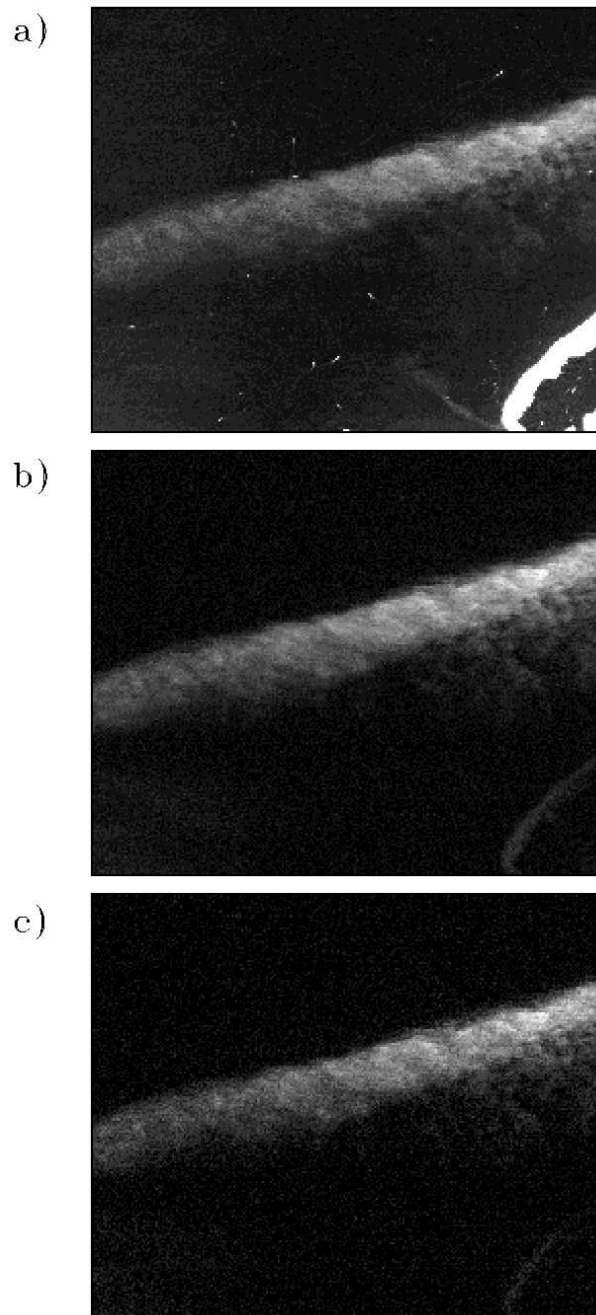


Fig. 22. AVIRIS Scene 1 images. (a) 1.24 μm image for Scene 1. (b) 1.38 μm image for Scene 1. (c) 1.88 μm image for Scene 1.

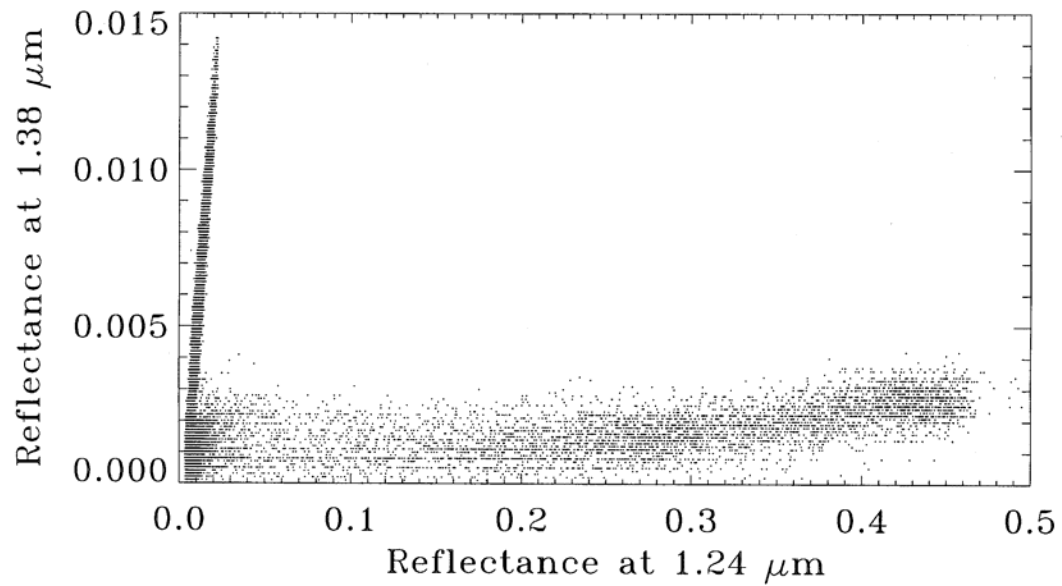


Fig. 23. Scene 1 AVIRIS 1.38 vs. 1.24 μm scatter plot. Note the horizontal swath of data points at the bottom of the plot, corresponding to low-level water clouds and surface effects. The steep, narrow swath of points on the left side of the plot indicates cirrus clouds.

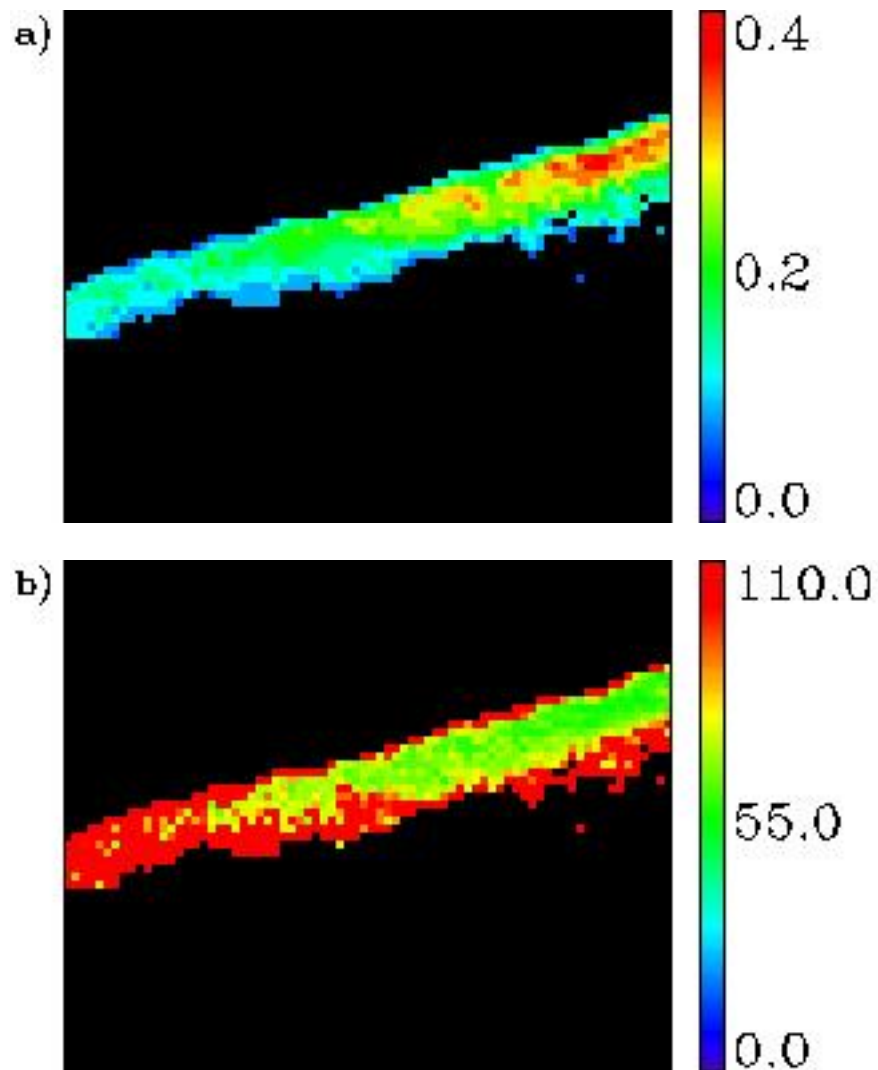


Fig. 24. Scene 1 retrieval images. (a) Retrieved cloud optical thickness corresponding to the images in Fig. 22. (b) Retrieved ice crystal effective diameter corresponding to Fig. 22.

Fig. 24 (a) shows the retrieved cloud optical thickness of the scene in Fig. 22. The plot range is scaled from 0.0 to 0.4, as displayed on the color bar. The retrieved optical thickness values indicate the very thin nature of this contrail cirrus cloud. The overall pattern of the image clearly matches that of Figs. 22 (a), 22 (b), and 22 (c). As expected, the largest values of optical thickness are found in the middle portion of the contrail cirrus.

Fig. 24 (b) shows the retrieved ice crystal effective diameter of the scene in Fig. 22. The plot range is scaled from 0.0 to 110.0 μm . Again, the overall pattern of the image clearly matches that of Figs. 22 (a), 22 (b), and 22 (c). The smallest ice crystal sizes are generally found in the middle of the contrail cirrus (corresponding to large optical thickness values). This is due to a unique aspect of 1.88 μm channel reflectance in that smaller ice crystals reflect more radiation than larger ice crystals, as evidenced by the plot in Fig. 21 (b).

5.3.2 *Natural Cirrus (Scenes 2 and 3)*

Fig. 25 (a) shows the 1.24 μm channel image for the natural cirrus scene (Scene 2) Acquired over the coastal areas of New Jersey. The center of the image is located at approximately 39.47°N and 76.04°W. The entire scene appears to be covered solely by cirrus clouds, with no surface effects. Thick cirrus clouds are evident in the upper left-hand corner of the image. The remainder of the image is covered with relatively thin cirrus. Fig. 25 (b) shows the 1.38 μm channel image. This image is very similar to the

image in Fig. 25 (a). The 1.88 μm channel image is shown in Fig. 25 (c). This image also appears very similar to the images in Figs. 25 (a) and 25 (b).

Fig. 26 shows the scatter plot of the 1.38 μm channel apparent reflectance values ($r^*_{1.375}$) versus the 1.24 μm channel apparent reflectance values ($r^*_{1.24}$) for AVIRIS Scene 2. Due to the lack of surface and lower level water cloud contributions to the 1.24 μm channel, all the pixels within the scene are very well clustered around a straight line having a slope of approximately 0.9. This slope is the best estimate of the water vapor transmittance ($T_{1.375}$) for the 1.375 μm channel.

Fig. 27 (a) shows the retrieved cirrus optical thickness for AVIRIS Scene 2. The plotted range is scaled from 0.0 to 2.0, as displayed on the color bar. The overall pattern of the image clearly matches that of Figs. 25 (a), 25 (b), and 25 (c). Maximum values of optical thickness are found in the upper left-hand portion of the plot, corresponding to the areas of high reflectance values in Figs. 25 (a), 25 (b), and 25 (c). Smaller optical thickness values are found in the remainder of the image. Unlike the contrail cirrus scene described above, this AVIRIS scene displays a thicker layer of cirrus clouds.

Fig. 27 (b) shows the retrieved ice crystal effective diameter for AVIRIS Scene 2. The plotted range is scaled from 0.0 to 60.0 μm , as displayed on the color bar. The overall pattern of this image is much harder to discern than that in Fig. 27 (a). However, as should be expected, smaller ice crystals are found in regions of higher cirrus reflectance (and thus larger optical thickness), as evident in the upper left-hand corner of the image. Relatively larger ice crystals comprise the remainder of the image

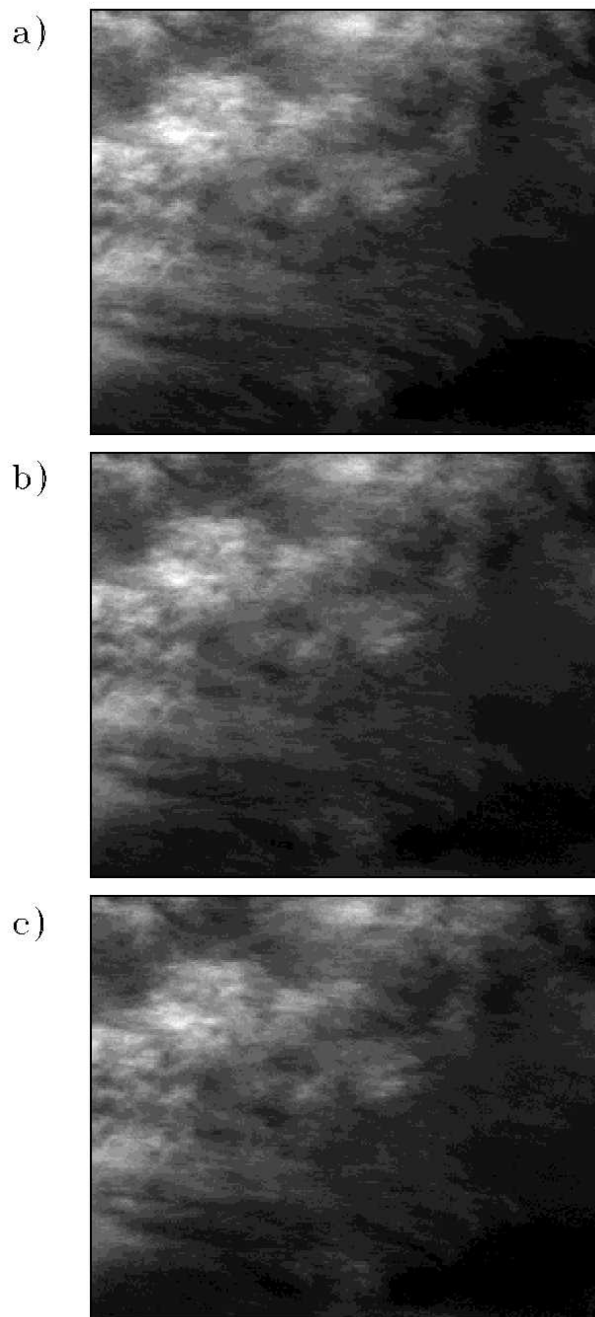


Fig. 25. AVIRIS Scene 2 images. (a) $1.24 \mu\text{m}$ image for Scene 2. (b) $1.38 \mu\text{m}$ image for Scene 2. (c) $1.88 \mu\text{m}$ image for Scene 2. Note the similarities between all three images.

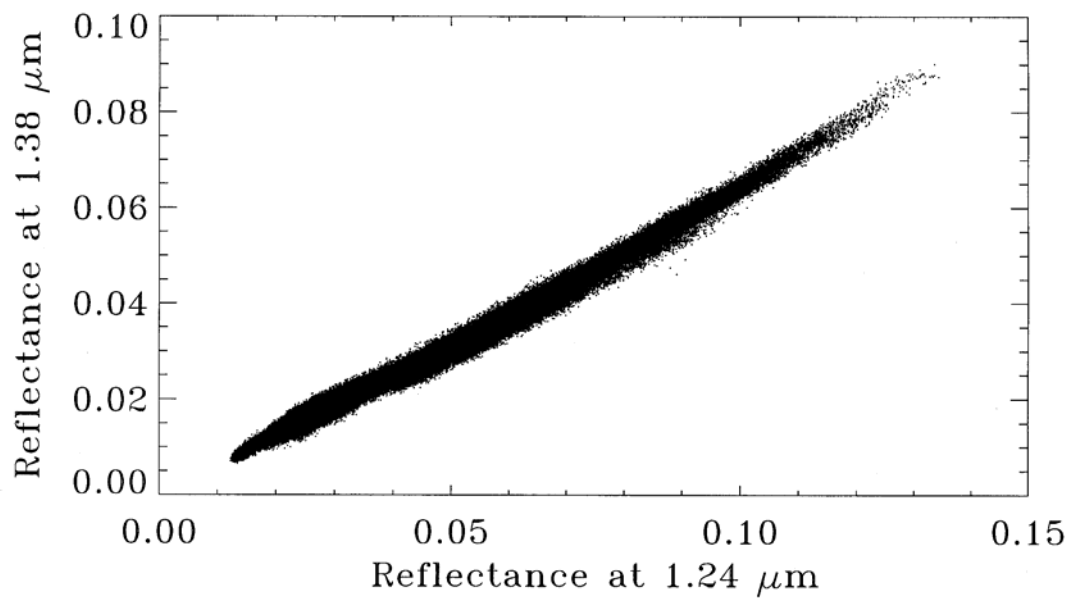


Fig. 26. Scene 2 AVIRIS 1.38 vs. 1.24 μm scatter plot. Note that all data points are clustered in a single, narrow swath, indicating the presence of only cirrus clouds.

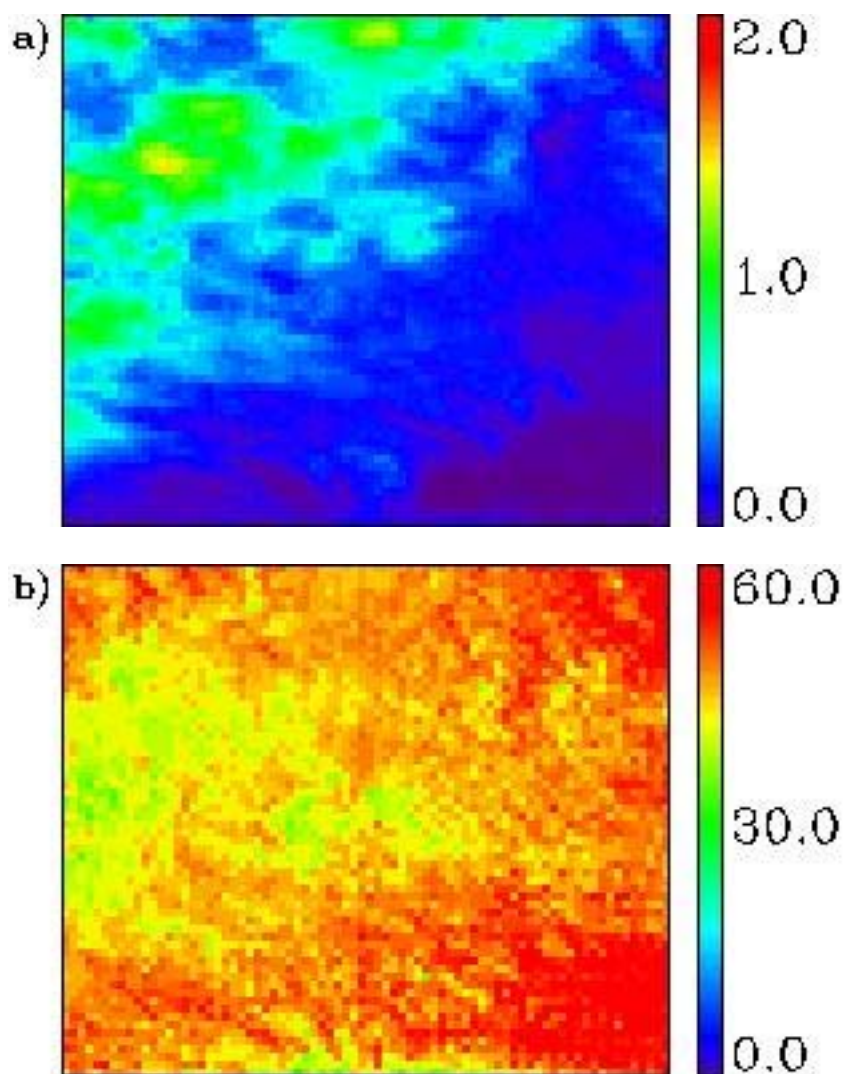


Fig. 27. Scene 2 retrieval images. (a) Retrieved cloud optical thickness corresponding to the images in Fig. 25. (b) Retrieved ice crystal effective diameter corresponding to Fig. 25.

(regions with lower cirrus reflectance). Overall, the retrieved effective diameters in this cirrus image are much smaller than those retrieved for the thin cirrus contrail in Fig. 24 (b), as is expected.

Fig. 28 (a) shows the 1.24 μm channel image for the second natural cirrus scene (Scene 3) taken over Monterey Bay, California. The center of the image is located at approximately 36.83°N and 122.06°W. As in Scene 2, the entire scene appears to be solely covered by cirrus clouds, without apparent surface effects. Major portions of the scene are covered with thin cirrus clouds. The upper right portion contains slightly thicker cirrus clouds. The 1.38 μm channel image in Fig. 28 (b) is very similar to the Fig. 28 (a) image. Fig. 28 (c) is the 1.88 μm image corresponding to Fig. 28 (a). This image is not as crisp as the images in Figs. 28 (a) and 28 (b), due to greater noise in this channel, but still captures the overall pattern of the cloud cover. Thicker cirrus appears in the upper right-hand corner, and thin cirrus is clearly evident throughout the remainder of the scene.

Fig. 29 shows the scatter plot of the 1.375 μm channel apparent reflectance values ($r_{1.375}^*$) versus the 1.24 μm channel apparent reflectance values ($r_{1.24}^*$) for the scene in Fig. 28. Due to the lack of surface and lower level water cloud contributions to the 1.24 μm channel, all the pixels within the scene are very well clustered around a straight line having a slope of approximately 0.9. This slope is the best estimate of the water vapor transmittance ($T_{1.375}$) for the 1.375 μm channel. The derivations of the intrinsic cirrus reflectance values for the 1.375 μm channel ($r_{1.375}$) and the 1.88- μm channel ($r_{1.88}$)

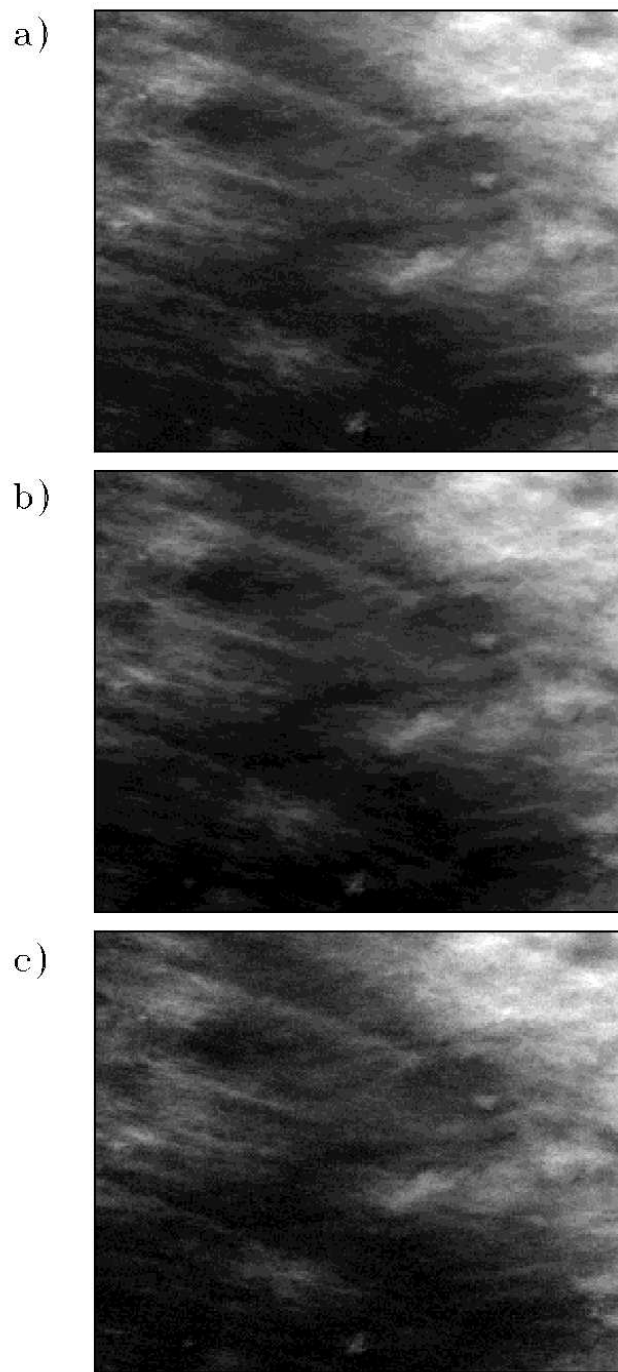


Fig. 28. AVIRIS Scene 3 images. (a) 1.24 μm image for Scene 3. (b) 1.38 μm image for Scene 3. (c) 1.88 μm image for Scene 3.

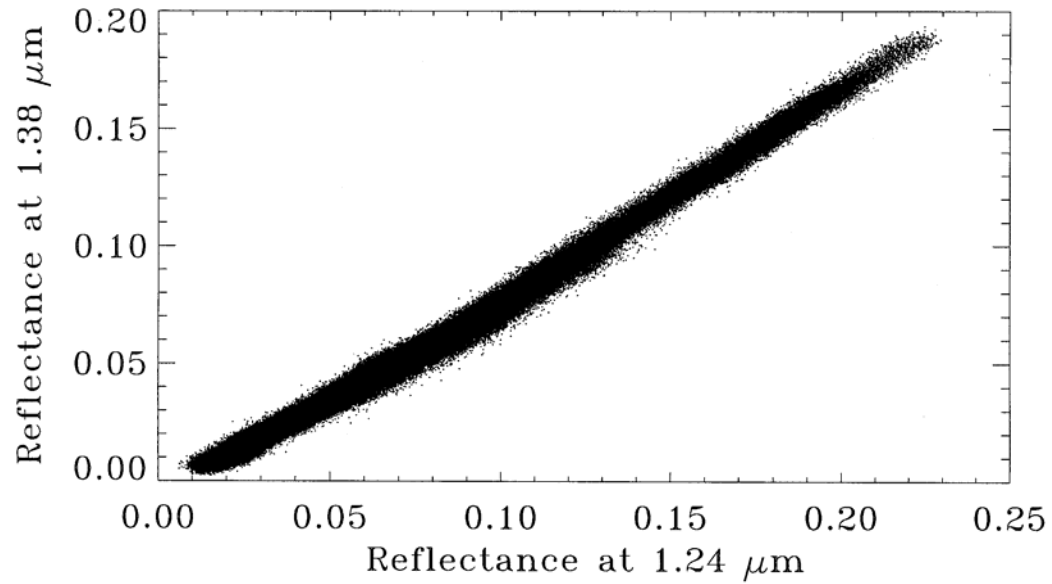


Fig. 29. Scene 3 AVIRIS 1.38 vs. 1.24 μm scatter plot. Note that all data points are clustered in a single, narrow swath, indicating the presence of only cirrus clouds.

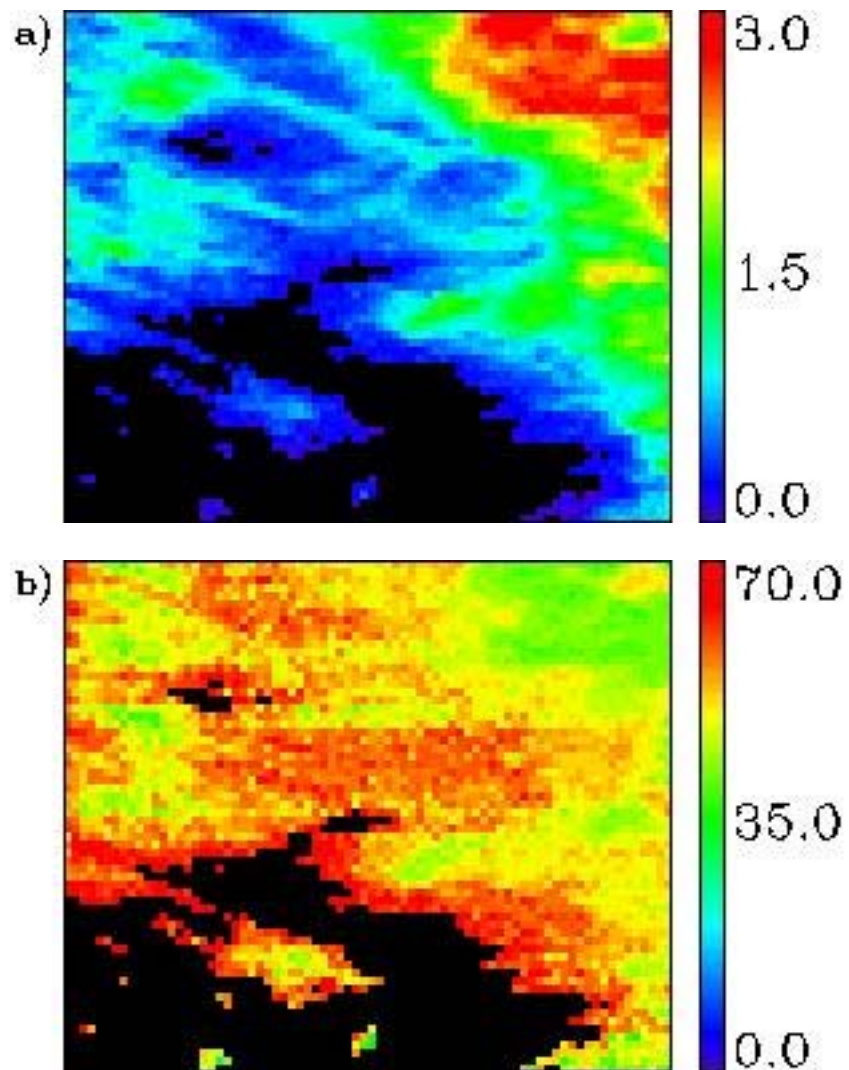


Fig. 30. Scene 3 retrieval images. (a) Retrieved cloud optical thickness corresponding to images in Fig. 28. (b) Retrieved ice crystal effective diameter corresponding to Fig. 28.

are then made using the techniques described in Section 5.2. In order to improve the signal to noise ratios of the intrinsic cirrus reflectances, a spatial averaging of the data is performed. The resulting data set has 76 x 64 pixels. The scatter plot of $r_{1.88}$ versus $r_{1.375}$ for the spatially averaged data is superposed over the curves generated from the simulated lookup tables, as shown in Fig. 21 (b).

The reflectance data in this case was collected before the upgrade to the AVIRIS instrument. Therefore, a lower threshold value of 0.02 on 1.88 μm channel reflectance data is applied. All 1.88 μm channel reflectance values below this threshold, as well as the corresponding 1.375 μm channel reflectance values, are assumed to be zero (i.e., clear-sky). This is done as a quality-control method to remove noise from the data.

Fig. 30 (a) shows the retrieved cloud optical thickness for the scene in Fig. 28. The plotted range is scaled from 0.0 to 3.0, as displayed on the color bar. The overall pattern matches that of Figs. 28 (a), 28 (b), and 28 (c). The large, red region of the image corresponds to the region of high reflectance in the upper right-hand corners of Figs. 28 (a), 28 (b), and 28 (c). Note that the lower left-hand corner has no retrieved optical thickness. This is a result of the threshold set on the 1.88 μm channel reflectance data to remove noise.

Fig. 30 (b) shows the retrieved ice crystal effective diameter of the scene in Fig. 28. The plotted range is scaled from 0.0 to 70.0 μm . Again, the overall pattern matches that of Figs. 28 (a), 28 (b), and 28 (c). Note the relatively small retrieved effective diameters in the region of high cirrus reflectance (upper right-hand corner). This is due to the characteristics of the 1.88 μm channel reflectance in that larger reflectance values

correspond to smaller ice crystal sizes. Also note the lack of retrieved effective diameter in the lower left-hand corner of the image, again due to the threshold set on the 1.88 μm channel reflectance data.

5.4 Discussion/Summary

Although a narrow 1.88 μm channel with a width of 30 nm is marked in Fig. 19 for remote sensing of cirrus optical properties, the center position and width of the channel should be further refined for implementation of the channel on possible future multi-channel meteorological satellite sensors. The atmospheric water vapor absorption and ice particle absorption effects vary rapidly with wavelength in the 1.7-2.1 μm spectral range. More systematic sensitivity and trade off studies are needed in order to optimize the selection of the center position and width of the channel.

Through analysis of hyperspectral imaging data collected with the AVIRIS instrument, a new concept has been established on the simultaneous retrieval of cirrus optical depth and effective ice particle diameter using narrow channels located within the 1.38 and 1.88 μm strong atmospheric water vapor band absorption regions. The theoretically simulated sensitivity curves in Fig. 21 indicate the validity of the new concept. Preliminary tests of the new concept with three sets of AVIRIS data have been made. Quite reasonable optical depths and effective ice particle sizes have been obtained. The implementation of the 1.375 μm channel on MODIS has enabled reliable detection of cirrus clouds on the global scale. It is anticipated that, if an additional narrow channel near 1.88 μm is implemented on a future multi-channel meteorological

satellite sensor, the ability to remotely sense cirrus optical depths and effective ice particle sizes on a global scale will be improved significantly.

6. SUMMARY AND CONCLUSIONS

Cirrus clouds play an important role in the earth's radiative processes, yet are one of the least understood components of the atmosphere. As a result, this topic has received a significant amount of focus from the atmospheric sciences community. With the development of the Airborne Visible Infrared Imaging Spectrometer (AVIRIS) in the early 1990s, cirrus cloud research gained a valuable instrument for various experiments. These studies led to the inclusion of the 1.375 μm "cirrus detection" channel [12] on the Moderate Infrared Spectroradiometer (MODIS) onboard both NASA's Terra and Aqua satellites. As a result, cirrus researchers now have an unprecedented view of global cirrus cover. Yet, much more needs to be done.

It is to this end that the research presented here is focused. First, a new method is introduced to retrieve tropical cirrus optical thickness from MODIS level-1b data using derived visible cirrus reflectance values with a look-up table approach. Visible cirrus reflectance is derived with the algorithm of Gao et al. [14], which uses a combination of the 0.66 and 1.375 μm MODIS channels. This new method can, theoretically, retrieve sub-visual cirrus clouds (i.e., cirrus clouds with optical thickness less than 0.03). However, this depends on the sensitivity of the MODIS data to thin cirrus clouds. It is also useful as a companion to the operational MODIS cloud retrieval algorithm for the case of cirrus clouds. Used together, cirrus can be removed from the operational MODIS optical thickness data to reveal low-level water clouds, which is especially useful in the case of mixed layer clouds.

The optical thickness retrieval algorithm, originally developed to operate on MODIS level-1b data, can be modified to operate on level-3 daily gridded data to provide a global view of cirrus cover. MODIS level-3 data contains the derived visible cirrus reflectance, which can be input directly into the algorithm. Using this data, statistical and climatological analyses can be performed. It is hoped that as the MODIS data set continues to grow, more statistically sound studies can be performed, resulting in a greater understanding of cirrus clouds and the roles they play in the radiation budget and climate.

Finally, a new method is introduced to retrieve cirrus optical thickness and ice crystal effective diameter simultaneously. This new method uses the 1.375 and 1.88 μm water vapor absorption bands, together with a visible channel, for the retrieval. Reflectance data for these channels are obtained from AVIRIS. A look-up table approach similar to the MODIS optical thickness retrieval is used. Quite reasonable results are produced. It is hoped that a new 1.88 μm channel can be included in upcoming NASA satellite missions for a more comprehensive study of cirrus clouds.

7. REFERENCES

- [1] B. A. Baum, D. P. Kratz, P. Yang, S. C. Ou, Y. Hu, P. F. Soulen, and S. -C. Tsay, “Remote sensing of cloud properties using MODIS airborne simulator imagery during SUCCESS, 1, Data and models,” *J. Geophys. Res.*, *105*, 11767-11780, 2000.
- [2] B. A. Baum, P. F. Soulen, K. I. Strabala, M. D. King, S. A. Ackerman, W. P. Menzel, and P. Yang, “Remote sensing of cloud properties using MODIS airborne simulator imagery during SUCCESS, 2, Cloud thermodynamic phase,” *J. Geophys. Res.*, *105*, 11781-11792, 2000.
- [3] S. Chandrasekhar, *Radiative Transfer*. New York: Dover.
- [4] H. Chepfer, G. Brogniez, and Y. Fouquart, “Cirrus clouds microphysical properties deduced from POLDER observations,” *J. Quant. Spectrosc. Radiat. Transfer*, *60*, 375-390, 1998.
- [5] H. Chepfer, P. Goloub, J. Spinhirne, P. H. Flamant, M. Lavorato, L. Sauvage, G. Brogniez, and J. Pelon, “Cirrus cloud properties derived from POLDER-1/ADEOS polarized radiances: First validation using ground-based lidar network,” *J. Appl. Meteor.*, *39*, 154-168, 2000.
- [6] C. O. Davis, J. Bowles, R. A. Leathers, D. Korwan, T. V. Downes, W. A. Snyder, W. J. Rhea, W. Chen, J. Fisher, W. P. Bissett, and R. A. Reisse, “Ocean PHILLS

- hyperspectral imager: Design, characterization, and calibration”, *Optics Express*, *10*, 210-221, 2002.
- [7] A. E. Dessler and P. Yang, “The distribution of tropical thin cirrus clouds inferred from Terra MODIS data,” *J. Climate*, *16*, 1241-1248, 2003.
- [8] J. S. Foot, “Some observations of the optical properties of clouds: II Cirrus,” *Quart. J. Roy. Meteor. Soc.*, *114*, 145-164, 1988.
- [9] P. N. Francis, A. Jones, R. W. Saunders, K. P. Shine, A. Slingo, and Z. Sun, “An observational and theoretical study of the radiative properties of cirrus: Some results from ICE’89,” *Quart. J. Roy. Meteor. Soc.*, *120*, 809-848, 1994.
- [10] Q. Fu, “An accurate parameterization of the solar radiative properties of cirrus clouds for climate models,” *J. Clim.*, *9*, 2058-2082, 1996.
- [11] B.-C. Gao, K. H. Heidebrecht, and A. F. H. Goetz, “Derivation of scaled surface reflectances from AVIRIS data,” *Remote Sens. Env.*, *44*, 165-178, 1993.
- [12] B.-C. Gao, and Y. J. Kaufman, “Selection of the 1.375- μm MODIS channel for remote sensing of cirrus clouds and stratospheric aerosols from space,” *J. Atm. Sci.*, *52*, 4231-4237, 1995.
- [13] B. -C. Gao, Y. J. Kaufman, W. Han, and W. J. Wiscombe, “Correction of thin cirrus path radiance in the 0.4-1.0 μm spectral region using the sensitive 1.375 μm cirrus detecting channel,” *J. Geophys. Res.*, *103*, 32169-32176, 1998.

- [14] B. -C. Gao, P. Yang, W. Han, R.-R. Li, and W. J. Wiscombe, "An algorithm using visible and 1.375- μm channels to retrieve cirrus cloud reflectances from aircraft and satellite data," *IEEE Trans. Geosci. Remote Sensing*, 40, 1659-1688, 2002.
- [15] B. -C. Gao, K. Meyer, and P. Yang, "A new concept on remote sensing of cirrus optical depth and effective ice particle size using strong water vapor absorption channels near 1.38 and 1.88 μm ," *IEEE Trans. Geosci. Remote Sensing*, 2004 (submitted).
- [16] R. O. Green, M. L. Eastwood, C. M. Sarture, T. G. Chrien, M. Aronsson, B. J. Chippendale, J. A. Faust, B. E. Parvi, C. J. Chovit, M. Solis, M. R. Olah, and O. Williams, "Imaging spectrometry and the Airborne Visible/Infrared Imaging Spectrometer (AVIRIS)", *Remote Sens. Env.*, 65, 227-248, 1998.
- [17] D. L. Hartmann, J.R. Holton, and Q. Fu, "The heat balance of the tropical tropopause, cirrus and stratospheric dehydration," *Geophys. Res. Lett.*, 28, 1969-1972, 2001.
- [18] D. L. Hartmann, and K. Larson, "An important constraint on tropical cloud - climate feedback," *Geophys. Res. Lett.*, 29, 2799-2802, 2002.
- [19] A. J. Heymsfield and G.M. Mcfarquhar, "A dedicated cloud microphysics mission during the Central Equatorial Pacific Experiment (CEPEX)," *Eighth Conf. On Atmospheric Radiation*, Nashville, TN, *Amer. Meteor. Soc.*, 166-168, 1994.
- [20] Y. -X. Hu, B. Wielicki, B. Lin, G. Gibson, S.-C. Tsay, K. Stamnes, and T. Wong, "δ-Fit: A fast and accurate treatment of particle scattering phase functions with

- weighted singular-value decomposition least-squares fitting,” *J. Quant. Spect. Radiative Transfer*, *65*, 681-690, 2000.
- [21] E. J. Jensen, O. B. Toon, L. Pfister, and H. B. Selkirk, “Dehydration of upper troposphere and lower stratosphere by subvisible cirrus clouds near the tropical tropopause,” *Geophys. Res. Lett.*, *23*, 825-828, 1996.
- [22] M. D. King, Y. J. Kaufman, W. P. Menzel, and D. Tanre, “Remote sensing of cloud, aerosol and water vapor properties from the Moderate Resolution Imaging Spectrometer (MODIS),” *IEEE Trans. Geosci. Remote Sensing*, *30*, 2-27, 1992.
- [23] M. D. King, S. -C. Tsay, S. E. Platnick, M. Wang, and K. N. Liou, “Cloud retrieval algorithms for MODIS: Optical thickness, effective particle radius and thermodynamic phase,” *MODIS Algorithm Theoretical Basis Document*, NASA, 1997.
- [24] M. D. King, W. P. Menzel, Y. J. Kaufman, D. Tanre, B. -C. Gao, S. Platnick, S. A. Ackerman, L. A. Remer, R. Pincus, and P. A. Hubanks, “Cloud and aerosol properties, precipitable water, and profiles of temperature and water vapor from MODIS,” *IEEE Trans. Geosci. Remote Sensing*, *41*, 442-458, 2003.
- [25] L. Kou, D. Labrie, and P. Chylek, “Refractive indices of water and ice in the 0.65- to 2.5- μm spectral range,” *Appl. Opt.*, *32*, 3531-3540, 1993.
- [26] A. Macke, J. Mueller, and E. Raschke, “Single scattering properties of atmospheric ice crystals,” *J. Atmos. Sci.*, *53*, 2813-2825, 1996.

- [27] J. H. Mather, T. P. Ackerman, M. P. Jensen, and W. E. Clements, "Characteristics of the atmospheric state and the surface radiation budget at the tropical western pacific ARM site," *Geophys. Res. Lett.*, *25*, 4513-4516, 1998.
- [28] G. M. McFarquhar, and A. J. Heymsfield, "Microphysical characteristics of three anvils sampled during the Central Equatorial Pacific Experiment (CEPEX)," *J. Atmos. Sci.*, *53*, 2401-2423, 1996.
- [29] G. M. McFarquhar, "Comments on 'Parameterization of effective sizes of cirrus-cloud particles and its verification against observations' by Zhian Sunand Lawrie Rikus (October B, 1999, 125, 3037-3055)," *Quart. J. Roy. Meteor. Soc.*, *126*, 261-266, 2000.
- [30] G. M. McFarquhar, P. Yang, A. Macke, and A. J. Baran, "A new parameterization of single scattering solar radiative properties for tropical anvils using observed ice crystal size and shape distributions," *J. Atmos. Sci.*, *59*, 2458-2478, 2002.
- [31] K. Meyer, P. Yang, and B.-C. Gao, "Optical thickness of tropical cirrus clouds derived from the MODIS 0.66- and 1.375- μm channels," *IEEE Trans. Geosci. Remote Sensing*, *42*, 2004.
- [32] T. Nakajima, and M. D. King, "Determination of the optical thickness and effective particle radius of clouds from reflected solar radiation measurements," *J. Atmos. Sci.*, *47*, 1878-1893, 1990.

- [33] S. L. Nasiri, B. A. Baum, A. J. Heymsfield, P. Yang, M. R. Poellot, D. P. Kratz, and Y. Hu, "The development of midlatitude cirrus models for MODIS using FIRE-I, FIRE-II, and ARM in situ data," *J. Appl. Meteor.*, *41*, 197-217, 2002.
- [34] S. Platnick, M. D. King, S. A. Ackerman, W. P. Menzel, B. A. Baum, J. C. Riedi, and R. A. Frey, "The MODIS cloud products: Algorithms and examples from Terra," *IEEE Trans. Geosci. Remote Sensing*, *41*, 459-473, 2003.
- [35] C. Prabhakara, D. P. Kratz, J.-M. Yoo, G. Dalu, and A. Vernekar, "Optically thin cirrus clouds: Radiative impact on the warm pool," *J. Quant. Spectrosc. Radiat. Transfer*, *49*, 467-483, 1993.
- [36] W. B. Rossow and R. A. Schiffer, "ISCCP cloud data products," *Bull. Am. Meteorol. Soc.*, *72*, 2-20, 1991.
- [37] L. S. Rothman, C. P. Rinsland, A. Goldman, S. T. Messie, D. P. Edwards, J. M. Flaud, A. Perri, C. Camy-Peyret, V. Dana, J. Y. Mandin, J. Schroeder, A. McCann, R. R. Gamach, R. B. Wattson, K. Yoshino, K. V. Chance, K. W. Jucks, L. R. Brown, V. Nemtchinov, and P. Varanasi, "The HITRAN molecular spectroscopic database and HAWKS (HITRAN Atmospheric Workstation): 1996 edition," *J. Quant. Spectrosc. Radiat. Transfer*, *60*, 665-710, 1998.
- [38] K. Sassen and B. S. Cho, "Subvisual-thin cirrus lidar dataset for satellite verification and climatological research," *J. Appl. Meteor.*, *31*, 1275-1285, 1992.

- [39] K. Stamnes, S.-C. Tsay, W. Wiscombe, and K. Jayaweera, "Numerically stable algorithm for discrete-ordinate-method radiative transfer in multiple scattering and emitting layered media," *Appl. Opt.*, *27*, 2502-2509, 1988.
- [40] G. Vane, R. O. Green, T. G. Chrien, H. T. Enmark, E. G. Hansen, and W. M. Porter, "The Airborne Visible/Infrared Imaging Spectrometer," *Remote Sens. Env.*, *44*, 127-143, 1993.
- [41] C. J. von Alt, M.P. De Luca, S.M. Glenn, J.F. Grassle, and D.B. Haidvogel, "LEO-15: Monitoring and managing coastal resources," *Sea Technology*, *38*, 10-16, 1997.
- [42] P. -H. Wang, M.P. McCormick, L. R. Poole, W. P. Chu, G. K. Yue, G. S. Kent, and K. M. Skeens, "Tropical high cloud characteristics derived from SAGE II extinction measurements," *Atmos. Res.*, *34*, 53-83, 1994.
- [43] P. -H. Wang, P. Minnis, M. P. McCormick, G.S. Kent and K. M. Skeens, "A 6-year climatology of cloud occurrence frequency from Stratospheric Aerosol and gas Experiment II observations (1985-1990)," *J. Geophys. Res.*, *101*, 29407-29429, 1996.
- [44] S. G. Warren, "Optical constants of ice from the ultraviolet to the microwave," *Appl. Opt.*, *23*, 1206-1225, 1984.
- [45] D. M. Winker and C. R. Trepte, "Laminar cirrus observed near the tropical tropopause by LIFE," *Geophys. Res. Lett.*, *25*, 3351-3354, 1998.

- [46] W. Wiscombe, "The delta- M method: Rapid yet accurate radiative flux calculations for strongly asymmetric phase functions," *J. Atmos. Sci.*, *34*, 1408-1422, 1977.
- [47] D. P. Wylie, W. P. Menzel, H. M. Woolf, and K. L. Strabala, "Four years of global cirrus cloud statistics using HIRS," *J. Clim.*, *7*, 1972-1986, 1994.
- [48] P. Yang and K. N. Liou, "Single-scattering properties of complex ice crystals in terrestrial atmosphere," *Contr. Atmos. Phys.*, *71*, 223-248, 1998.
- [49] P. Yang, K. N. Liou, K. Wyser, and D. Mitchell, "Parameterization of the scattering and absorption properties of individual ice crystals," *J. Geophys. Res.*, *105*, 4699-4718, 2000.

VITA

Biography

Kerry Glynn Meyer was born in Manhattan, KS, on July 27, 1979, and shortly after moved with his family to northern Indiana. He then moved to Midlothian, TX, in the summer of 1989, and has remained in the Lone Star State ever since. He graduated salutatorian from Midlothian High School in the spring of 1997, and enrolled in Texas A&M University as a freshman the following fall. His permanent address is 2251 Oak Tree Ln., Midlothian, TX 76065.

Educational Background

B.S., Meteorology , Texas A&M University, December 2001.

M.S., Atmospheric Sciences, Texas A&M University, May 2004.

Publications

K. Meyer, P. Yang, and B.-C. Gao, "Optical thickness of tropical cirrus clouds derived from the MODIS 0.66- and 1.375- μm channels," *IEEE Trans. Geosci. Remote Sensing*, 2004 (in press).

B. -C. Gao, K. Meyer, and P. Yang, "A new concept on remote sensing of cirrus optical depth and effective ice particle size using strong water vapor absorption channels near 1.38 and 1.88 μm ," *IEEE Trans. Geosci. Remote Sensing*, 2004 (submitted).